for Special Issue in the Journal of Polymer Science on "Emerging Characterization Techniques"

Title: Characterization of Polymeric Surfaces and Interfaces using Time-of-Flight Secondary Ion Mass Spectrometry

Hao Mei[1, †], Travis S. Laws[2, †], Tanguy Terlier[3], Rafael Verduzco [1,3,4,*], Gila E. Stein[2,*]

[1] Dr. Hao Mai, Prof. Rafael Verduzco, Department of Chemical and Biomolecular Engineering, Rice University, Houston, Texas 77005, United States

[2] Travis S. Laws, Prof. Gila E. Stein, Department of Chemical and Biomolecular Engineering, University of Tennessee, Knoxville, TN 37919, United States

[3] Dr. Tanguy Terlier, Prof. Rafael Verduzco, Shared Equipment Authority, Rice University, Houston, Texas 77005, United States

[4] Prof. Rafael Verduzco, Materials Science and NanoEngineering, Rice University, Houston, Texas 77005, United States

† Equal contribution.

*rafael@rice.edu, gstein4@utk.edu

Keywords: ToF-SIMS, time-of-flight secondary ion mass spectrometry, depth profiling, spectral analysis, imaging

Abstract: Time-of-flight secondary ion mass spectrometry (ToF-SIMS) is used for chemical analysis of surfaces. ToF-SIMS is a powerful tool for polymer science because it detects a broad mass range with good mass resolution, thereby distinguishing between polymers that have similar elemental compositions and/or the same types of functional groups. Chemical labeling techniques that enhance contrast, such as deuterating or staining one constituent, are generally unnecessary. ToF-SIMS can generate both two-dimensional images and three-dimensional depth profiles, where each pixel in an image is associated with a complete mass spectrum. This Review begins by introducing the principles of ToF-SIMS measurements, including instrumentation, modes of operation, strategies for data analysis, and strengths/limitations when characterizing polymer surfaces. The sections that follow describe applications in polymer science that benefit from characterization by ToF-SIMS, including thin films and coatings, polymer blends, composites, and electronic materials. The examples selected for discussion showcase the three standard modes of operation (spectral analysis, imaging, and depth profiling) and highlight practical considerations that relate to experimental design and data processing. We conclude with brief comments about broader opportunities for ToF-SIMS in polymer science.

Introduction

In the first 100 years of polymer science, we have witnessed remarkable advances and achievements in the development and understanding of polymeric materials. This includes work in advancing polymer chemistry, physics, modelling, and simulations. However, these advances would not have been possible without the development of techniques capable of characterizing polymeric materials across multiple length scales. Imaging techniques such as transmission electron microscopy (TEM) and scanning electron microscopy (SEM) provide real-space images of structural features down to nanometer length scales. X-ray and neutron scattering techniques provide information on molecular-level and meso-scale ordering and structure. Rheological measurements are critical to understanding flow and deformation of polymeric materials across multiple time scales, and atomic force microscopy (AFM) can provide information on both structure and mechanics at surfaces. Surface analysis techniques such as X-ray photoelectron spectroscopy (XPS) and secondary ion mass spectrometry (SIMS) provide insight into surface chemistry along with morphological information. This list of techniques is not comprehensive, and other important characterization techniques applied to polymeric materials include dielectric spectroscopy, differential scanning calorimetry, spectroscopic ellipsometry, optical microscopy, and quartz-crystal microbalance dissipation spectroscopy, among others. The variety of characterization techniques commonly used in polymer science reflects the complexity of polymeric materials. In general, no single technique can provide sufficient feedback on structure, chemistry, mechanics and dynamics, and therefore multiple complementary characterization techniques are needed.

Time of flight secondary ion mass spectrometry (ToF-SIMS) utilizes a focused ion beam to sputter atoms and molecular fragments from a surface. A fraction of these sputtered atoms and molecular fragments are sent to a time-of-flight detector, which determines their molecular weight with good resolution. The focused ion beam provides spatially resolved information on the surface, and when paired with a secondary beam for depth profiling, ToF-SIMS can provide three-dimensional information on polymer chemistry. The unique capabilities of ToF-SIMS complement those of more commonly used techniques in polymer science, and ToF-SIMS can provide critical insight to advance the development of polymers for various key applications. ToF-SIMS is used regularly in industry as an analytical technique to identify potential contaminants on a surface or understand differences in surface chemistry that may influence adhesion, wetting, biological integration, catalyst fouling, or other performance characteristics.[1–4] As an example, ToF-SIMS has been used in the polymers industry to quantify the surface composition of ethylene/propylene copolymers and blends.[5] However, as a tool for academic polymer research, ToF-SIMS is far less common than scattering techniques, XPS, and AFM. This is likely due to a combination of

factors, including limited access to ToF-SIMS instrumentation, unfamiliarity with the technique, and specific limitations of the ToF-SIMS technique. Over the past 10 – 20 years, ToF-SIMS has become more widely accessible, and the technique has advanced in several significant ways that are relevant to the study of polymers and soft materials. For example, the use of gas cluster beams has improved the depth resolution for etching of soft materials, enabling sub-20 nm depth resolution in the analysis of polymer films.

The goal of this review is to provide an overview of ToF-SIMS for the polymer science community. We start with an overview of the technique and introduce the three standard measurement modes (spectral analysis, imaging, depth profiling), highlighting both the strengths and limitations of the method. We then discuss examples from the literature on the application of ToF-SIMS to polymeric films and coatings, polymer blends, polymer composites, and electronic materials and devices. We conclude with a brief perspective on the potential of ToF-SIMS for advancing current areas of interest to the polymer science community. This review is intended as an introduction to ToF-SIMS for researchers in the polymer science community and is not a comprehensive review of ToF-SIMS. For more in-depth information on instrumentation and principles of ToF-SIMS, we refer the reader to other textbooks[6–8] and review articles[9–11].

Section 2: Overview of ToF-SIMS

2.1 Overview of ToF-SIMS and Comparison to Dynamic SIMS

Secondary ion mass spectrometry (SIMS) is a surface analysis technique that provides spatially resolved information on the elemental and molecular chemistry of a surface. The technique involves bombardment of a surface with a focused ion beam, which results in the sputtering of a variety of particles from the surface including electrons, photons, and atomic and molecular species. The sputtering process and formation of secondary ions involves a transfer of kinetic energy through collisions between the ions in the primary beam and the molecules near the top of the surface[11]. While most of the sputtered atomic and molecular species are neutral, a fraction (typically much less than 1%) are charged and can be collected and analyzed. These charged species are known as secondary ions, and they reflect the chemistry of the target region of the surface[6,12].

SIMS techniques can be classified as either static or dynamic. In static SIMS, the primary beam current is operated below the static limit[6] (approximately 10^{13} ions/cm^2) to minimize damage to the surface during analysis. When operated in static mode, at most 1 % of the atoms on the surface are sputtered, and as a result the surface is not significantly etched or damaged during analysis. Conversely, dynamic SIMS uses much higher beam currents (approximately 10^{17} ions/cm^2), resulting in continuous etching (i.e., depth profiling) of the surface during analysis, and the primary beam is operated in direct current (DC) mode.

Dynamic SIMS produces much higher secondary ion fluxes, and as a result has better sensitivity (as low as 10^{13} atoms/cm^3) and a wider dynamic detection range (from 5×10^{22} atoms/cm^3 to 5×10^{12} atoms/cm^3). A drawback of dynamic SIMS is that only atomic or small molecular ionic species can be detected. While such fragments are useful in depth profiling of certain polymeric systems[13], a complete mass spectrum is needed to differentiate polymers that have similar chemical structures, among other scenarios that are discussed herein. This review is focused exclusively on ToF-SIMS and its applications in polymer science, and more detailed information about dynamic SIMS can be found in other publications.[6,14]

ToF-SIMS is a static SIMS technique in which the primary analysis beam is pulsed and secondary ions are analyzed using a time-of-flight (ToF) mass analyzer (Figure 1). Secondary ions are accelerated to a ToF spectrometer which records the mass-to-charge (m/z) ratios. The m/z ratios are determined by measuring the time required for ions to traverse the flight path from the surface to the detector. With knowledge of the flight path and the electrical potential, and assuming unit charge, the mass of the ion can be determined. Furthermore, the ToF mass analyzer can discriminate between ions with excellent mass resolving power[15–20]. The surface under analysis is not significantly etched by the primary beam, but the technique can be paired with a secondary beam (dual sputter gun) to perform a depth profiling analysis. ToF-SIMS therefore provides surface-sensitive analysis of a wide range of atomic and molecular fragment ions, and this is particularly useful for the analysis of polymeric and organic materials.

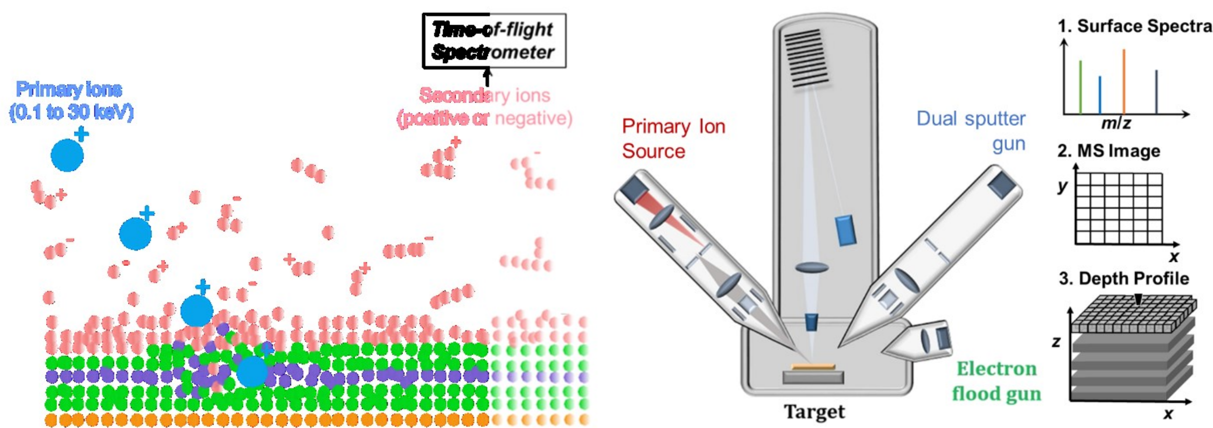

Figure 1: Schematic for analysis of a surface by ToF-SIMS showing (left) the sputtering process that generates secondary ions, (middle) an overview of the instrumentation, and (right) modes of analysis that include acquisition of a surface mass spectrum, a mass-spectrometry (MS) image, and a depth profile of the material which produces a 3-D volume rendered dataset. Each pixel contains a full-range mass spectrum for that region of the sample.

2.2 Components of the ToF-SIMS

Here, we briefly introduce the basic components of the ToF-SIMS, which include the primary ion beam and a beam for sample etching that enables depth profiling. (The ToF mass analyzer was described in the preceding section.) The primary beam is pulsed to enable analysis by a time-of-flight mass spectrometer. Liquid metal ion guns (LMIGs) based on bismuth are most used in commercial ToF-SIMS instruments. These can be operated at lower temperatures compared with other LMIG sources such as gold and can produce ion clusters (e.g. Bi_3^+) for analysis. These ion beams can also be tightly focused to achieve high spatial resolution (< 200 nm) and have excellent stability through the duration of a measurement. More information on primary ion sources is available in the literature.[21]

Subsurface analysis can be achieved by operating in dual beam mode, which involves alternating the primary ion beam used for analysis and a second, low-energy (typically between 100 eV to 20keV) and high-current beam for etching the sample. By using two beams, the advantages of LMIG for analysis are combined with capabilities for uniform etching with high depth resolution.[22] Cluster ions are particularly useful for depth-profiling of organic and soft materials because they do not penetrate far into the material, thereby preserving the structures underneath the surface[23,24]. Figure 2a presents snapshots of molecular dynamics simulations of argon cluster ions impacting a surface. As the cluster size increases, the damage is increasingly confined to the material surface[25,26]. A variety of polyatomic ions have been tested and implemented for depth profiling of soft materials, including SF_5^+ and C_{60}^{2+},[27,28] and large argon clusters have emerged as the best for quantitative depth profiling of soft materials.[24,29] The argon gas cluster ion source offers the possibility to tune the cluster size and the energy-per-atom ratio for improving the secondary ion signal intensity and depth resolution[24,30–33], and these are now available in commercial ToF-SIMS systems. Terlier et al. compared the performance of Cs^+, C_{60}^{2+}, and Ar_{1500}^+ in performing depth-profiling analysis of an aligned block copolymer film in a cylindrical morphology. The authors found much more uniform depth profiling using the polyatomic cluster ions compared with Cs^+.[34] Another study used Ar_{2000}^+ to perform depth profiling analysis of multilayer films containing up to 50 alternating layers of polystyrene (PS) and polyvinylpyrrolidone (PVP). The thicknesses of the layers ranged from 40 – 370 nm. By using Ar_{2000}^+ for etching, the authors were able to clearly resolve the layers, even for a 50-layer sample and total depth exceeding 15 µm, as shown in Figure 2b.[29] Another study compared the depth resolution of polyatomic argon clusters (Ar_{2000}^+ and Ar_{2500}^+) and C_{60}^{2+} by etching through multilayers of vacuum-deposited organic antioxidant stabilizers and found that argon clusters produced more uniform etching and better depth resolution, with full width at half maximum (fwhm) of 5 nm.[24]

The depth resolution depends on the material, cluster size, beam current, and the beam energy, and in general the depth resolution of ToF-SIMS is inferior to X-ray and neutron reflectivity. Depending on

sample chemistry and the type of sputter gun, the depth resolution can be improved through sample cooling and sample rotation. These points were examined through analysis of vacuum deposited alternating organic multilayers consisting of thick (approx. 50 nm) and thin (approx. 3 nm) antioxidant layers that can be readily distinguished by ToF-SIMS. Sjövall et al. demonstrated that either sample cooling (to -80 ºC) or sample rotation (at 14 Hz) was necessary to resolve each of the thin 'delta' layers in the sample when using C_{60}^{2+} for depth profiling. Without sample rotation or sufficient cooling, the depth resolution degraded significantly and the authors observed a decrease in sputtering yield with depth[35]. However, a similar follow-up study using Ar cluster ions (which is a commonly used source for polymer depth profiling) found that rotation or cooling were not needed to resolve the delta layers. Four laboratories working independently were able to clearly resolve each of the delta layers using Ar cluster ions for depth profiling, with a discrepancy of up to 3 nm in the positions of the delta layers[24].

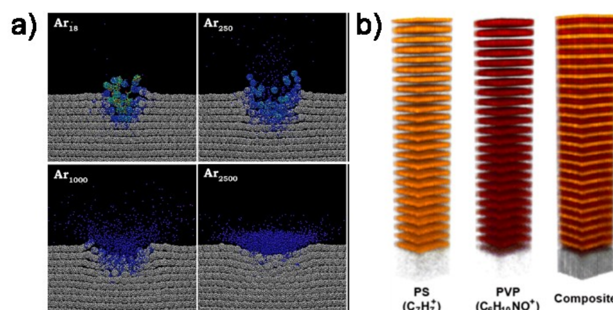

Figure 2: (a) Molecular dynamics simulations of cross-sectional and zoomed side view of the time evolution snapshots at 3 ps after bombardment with Ar_n (n = 18, 250, 1000 and 2500) cluster projectiles. Reproduced with permission from Ref. [36]. (b) False-color image of a ToF-SIMS depth profiling experiment using Ar_{2000}^+ cluster ions. The sample was comprised of 50 alternating layers of polystyrene and polyvinylpyrollidone, where each layer was approximately 300 nm thick, for a total sample thickness of 15 µm. Reproduced with permission from Ref. [29].

Other components of the ToF-SIMS instrument include the electrostatic reflectron mirror, the vacuum system, and an electron flood gun. A vacuum environment ($<10^{-8}$ mbar for modern instruments) is required to prevent surface contamination by removing volatile components, increase the mean free path of secondary ions, and enable high voltages without breakdown or discharges[6]. An electron flood gun is used to neutralize or minimize surface charge during analysis, and the electron flood gun is pulsed periodically

(approximately 1:10 duty cycle) with the AC primary beam. More detailed information on ToF-SIMS components and instrumentation can be found elsewhere.[6]

2.3 ToF SIMS modes of operation and analysis

There are three basic modes of analysis in ToF-SIMS: spectral analysis, imaging, and depth profiling, and examples of each are shown in Figure 3. Spectral analysis is the simplest and most common and involves acquiring a high-resolution mass spectrum for the surface under analysis. This can be used for a variety of purposes including identifying contaminants,[37,38] determining the relative abundances of elements or molecules,[39–42] studying the orientations of molecules on a surface,[43,44] or distinguishing between block and random copolymers.[45] For example, Liu et al. analyzed poly(styrene–*co*–4-vinyl phenol) (PS-P4VP) random and block copolymers matched in size and composition.[45] The spectrum for the random copolymer (Figure 3a**)** contained secondary ions that corresponded to either PS, P4VP, or both S and 4VP. Peaks at m/z = 183 and 209 were associated with S-4VP units and were only present in the spectra for the random copolymer. The spectra for the block copolymer only contained secondary ions for PS or P4VP fragments and not S-4VP units. ToF-SIMS analysis of these materials could therefore easily distinguish between the two types of copolymers. The authors also demonstrated that after calibration, they could quantitatively determine the ratio of S and 4VP in the random copolymers by analysis of the mass spectra.

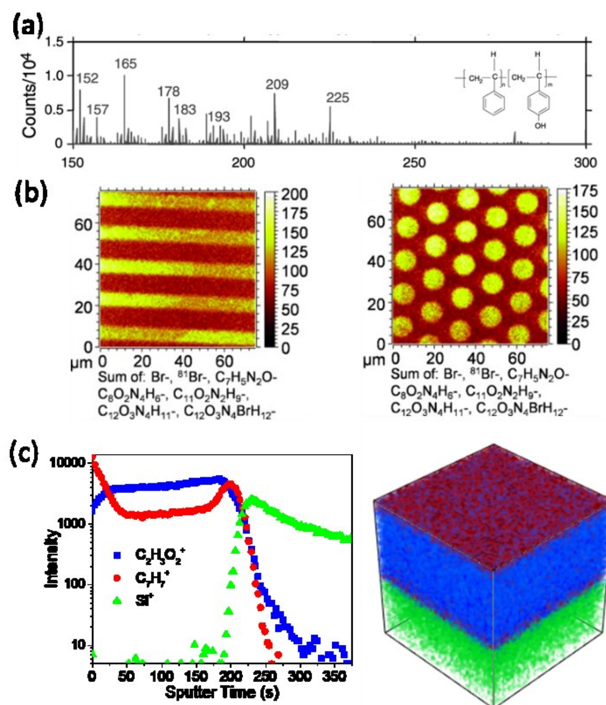

Figure 3: Examples of (a) spectral, (b) imaging, and (c) depth-profiling modes of ToF-SIMS analysis. (a) Positive ToF-SIMS spectrum of the PS-P4VP copolymer. Reproduced with permission from Ref. [45] (b) ToF-SIMS data of ATRP-TAD printed in 5 µm stripes spaced by 10 µm (left) and reprinted ATRP-TAD in 10 µm dots spaced by 5 µm (right). Reproduced with permission from Ref.[39] (c) Depth profiling of bottlebrush copolymer additives with polystyrene (PS) and poly(methyl methacrylate) (PMMA) side-chains in linear PMMA (left). The blue color reflects the $C_2H_3O_2^+$ from linear PMMA chains while the red reflects $C_7H_7^+$ ions from PS side chains in the bottlebrush copolymer additives. The green color reflects Si^+ from the silicon substrate. Reproduced with permission from Ref. [41].

In imaging mode, the primary beam is focused to enhance the lateral resolution and rastered across the surface to produce a mass spectral "image," and this can be used to characterize chemically-distinct regions on the surface. For example, Roling et al. produced a micropatterned surface using microcontact printing to deposit a self-assembled monolayer followed by surface-initiated polymerization to grow polymer brushes from the patterned regions. Figure 3b shows ion images of a patterned polymer brush film in either stripes or dots on a surface, depending on the stamp used. The polymer brush regions were easily distinguished from the surface by ToF-SIMS, and the lateral resolution was sufficient to clearly resolve the 5 µm stripes and 10 µm dots.[39] In this study, the aspect ratio of the patterns (height/width) was very low. However, when samples present with significant topography, the measurement is complicated by several

factors. As examples, the data from a rough surface are projected onto a 2D map, and the sputtering rate may differ across the surface due to variation in the angle of incidence of the primary ion beam, or due to spatial variations in composition.[46,47] Note that resolving lateral features on a surface that are smaller than 100 nm is not possible since this approaches the physical limits for detection of secondary ions. Furthermore, there is a trade-off between the spatial resolution and the mass resolving power that can be achieved in a single measurement. To achieve a high mass resolving power, the instrument is operated in "bunched" mode, which involves short pulses (approximately 600 ps)[9] of the primary ion beam. Conversely, high spatial resolution can be achieved using longer pulses (10 – 100 ns) in a "burst alignment" mode[9] at a cost of mass resolving power. Alternative modes to improve spatial resolution while maintaining good mass resolving power include using a series of short pulses ("burst mode") [9] or delayed extraction[48], but both of these methods involve trade-offs in terms of count rates and in the analysis of low-mass ions.

Depth profiling is achieved through dual beam mode, where an ion source separate from the primary ion beam is used to etch away the top surface of the material. This etching is alternated with the primary beam to produce mass spectra as a function of depth. This can also be combined with lateral imaging to produce three-dimensional mass spectrometry images. For example, Mei et al. analyzed polymer blends containing a linear poly(methyl methacrylate) (PMMA) and a surface-active PS-PMMA bottlebrush copolymer. To characterize these blend films, they performed ToF-SIMS depth profiling and measured the intensities of $C_7H_7^+$ and $C_2H_3O_2^+$ secondary ions, corresponding to PS and PMMA, respectively, as shown in Figure 3c. They were able to observe enrichment of the bottlebrush copolymer additive at the film surface (reflected in the higher $C_7H_7^+$ intensity at sputter time of 0), and they acquired a three-dimensional mass spectrometry image that clearly showed enrichment of the bottlebrush at the top of the film. The authors of this study were also able to perform a semi-quantitative analysis of blend composition as a function of depth by calibrating the ion intensities in homogeneous blends of known composition.[41] It is important to emphasize that knowledge of the sample chemistry is critical for an accurate ToF-SIMS depth profile, as a calibration curve is generally required to convert counts to composition.

Depth profiling by ToF-SIMS can provide similar information as neutron reflectivity (NR) and X-ray reflectivity (XRR), namely a depth-dependent composition. There are three features of ToF-SIMS depth profiling that arguably make this technique more accessible than reflectivity: 1) ToF-SIMS is highly sensitive to slight differences in chemical composition and does not require a deuterium label (common for NR measurements of polymers) or large electron density contrast (XRR). 2) Depth profiling by ToF-SIMS generates a real-space composition profile, while NR and XRR are reciprocal-space techniques that yield a real-space profile through modeling of the data. 3) Each ToF-SIMS measurement samples a small area, ca. 500 µm x 500 µm or smaller, and can be applied to ultrathin (~10 nm) or thick (~10 µm) films. The thickness

limit is partly set by practical considerations rather than instrumentation, as sputtering through tens of micrometers would take a very long time. (While cross-sectional imaging enabled by ultra-low-angle microtomy can probe the through-film structure in films that are 100s of micrometers thick, the lateral resolution of this technique is quite poor.) Reflectivity requires a large-area sample due to the long beam footprint and is generally limited to thin films (<500 nm).

A key disadvantage of ToF-SIMS is the limited depth resolution when applied to polymers, which means that sharp interfaces that should produce a step-function depth profile cannot be resolved. Instead, the apparent composition varies continuously across the interface, and the standard deviation (σ) of this profile depends on the sputtering source, the material chemistry, and the sputtered depth. This relatively poor depth resolution can be attributed to the matrix effect, which may alter the apparent shape and position of an interface, as well as to surface roughening that may increase with depth of sputtering. As examples, Figure 4 shows ToF-SIMS depth profiles for a thin film of PS-*b*-PMMA lamellae and for a bilayer of deuterated PS (dPS) and protonated PS, both on silicon substrates. Argon cluster ions were used for sputtering. The PS-*b*-PMMA lamellae assemble into well-defined layers through the film thickness, as evidenced by the periodic oscillation of the O^- signal which is unique to PMMA. Prior x-ray scattering studies of a nearly identical PS-*b*-PMMA showed that the interfacial width (between PS and PMMA domains) is approximately 5 nm, or $\sigma \approx 2$ nm, consistent with mean-field predictions.[49] However, the O^- oscillations in Figure 4a are significantly more smeared than expected, matching $\sigma \approx 8$ nm. A similar outcome is found for the dPS/PS bilayers that were prepared by floating a dPS film on top of a spun-cast PS film: while neutron reflectivity measures an interface with $\sigma = 3.6$ nm, ToF-SIMS depth profiling ($C_7D_7^+$ signal) detects an interface with $\sigma \approx 10$ nm, as shown in Figure 4b. We note that studies of model organic multilayers showed that depth profiling with Argon cluster ions could achieve a (best-case) depth resolution of $\sigma \approx 2$ nm that was constant through the thickness of a ca. 300 nm film.[24] Another important distinction between ToF-SIMS and NR or XRR is sample environment, as ToF-SIMS can only probe samples under vacuum while NR and XRR can also measure polymer/liquid interfaces.

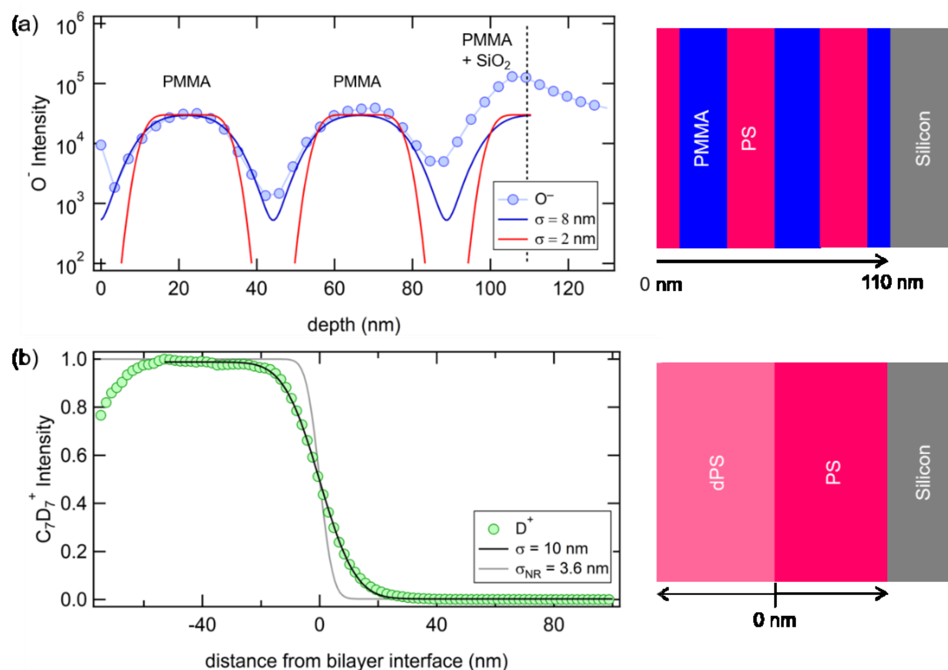

Figure 4: (a) PS-b-PMMA lamellae oriented parallel to the silicon substrate. The oxygen (O^-) signal is unique to PMMA domains (and the native oxide at the silicon substrate). The expected profile for this material is shown in red, and an approximate fit is shown in blue. The vertical dashed line marks the polymer/substrate interface. (b) dPS/PS bilayer. The best-fit profile to the deuterium signal ($C_7D_7^+$) is shown in black, and the profile determined through neutron reflectivity is shown in grey.

2.4 Challenges in ToF-SIMS data analysis

A significant drawback of the ToF-SIMS technique is that the secondary ion intensities measured do not directly correspond to the abundance of the corresponding elements or molecules on the surface, and therefore the method is generally not quantitative. The intensities of secondary ions generated depend on a variety of factors including chemical abundance, mass of the ion, and the so-called "matrix effect".[50] The matrix effect is observed when a fragmentation process is dependent on the types of chemical moieties within the polymer (end-group chemistry,[51] comonomer[52]) and/or noncovalent interactions such as hydrogen bonding[53]. For this reason, the secondary ion yield for a particular secondary ion can vary by orders of magnitude with changes in the local chemical environment. As an example, in random copolymers of styrene and methylmethacrylate, the absolute intensity of several styrenic fragments is higher than expected based on composition, and even higher than observed for polystyrene homopolymer[52]. Another example is blends of poly(styrene-co-4-vinylpyridine) and poly(styrene-co-4-vinylphenol), where proton transfer from phenolic to pyridinyl moieties enhances the intensity of pyridinyl ions relative to the

theoretical value based on sample composition.[53] The matrix effect is not unique to organic materials and is also observed in inorganic materials such as metallic alloys.[54]

Several techniques have been developed to minimize or eliminate the matrix effect and achieve semi-quantitative or quantitative analysis. Secondary ion intensities can be calibrated through analysis of well-defined standards, and in many examples the ratios of secondary ion intensities depend linearly on the relative composition of the atomic or molecular species at the surface,[11,40,41,45,55–59] even when a strong matrix effect is present.[55] For the spectrum shown in Figure 3a, the authors showed that secondary ion intensities corresponding to either PS or P4VP varied linearly with the composition of the random copolymer, and therefore ToF-SIMS could be used to quantify the copolymer compositions. For the blend study shown in Figure 3c, the authors were able to determine the depth dependent concentration of the blend by analyzing homogeneous blends of known composition to calibrate $C_7H_7^+$ and $C_2H_3O_2^+$ secondary ion intensities. Shard et al. studied blends of polylactide (PLA) with the small molecule drug codeine. They observed a strong matrix effect and an overall reduction of secondary ion intensity with increasing composition of codeine relative to PLA in the blend, but they were able to produce a linear calibration scale by measuring the ratios of secondary ion intensities corresponding to codeine and PLA. They also introduced a kinetic model for charge transfer that could account for the changes in the secondary ion intensities with changes in film composition[60]. In a follow up study, Shard et al. used an empirical expression to model the variations in secondary ion intensities as a function of the volume fraction of each component in a binary blend and defined a parameter to quantify the sign and magnitude of the matrix effect in blends[61]. Other approaches for semi-quantitative analysis include metal-assisted SIMS (MetA-SIMS), where a thin metal is deposited on top of the material under analysis,[62,63] analysis of prominent ion signals from metallic cations,[64,65] and laser post-ionization[66,67].

The large size of ToF-SIMS datasets can complicate analysis. ToF-SIMS datasets can include three-dimensional spatial information and high-resolution mass spectra, similar to hyperspectral image maps. A number of multivariate analysis (MVA) techniques have been used to analyze ToF-SIMS datasets, such as principal component analysis (PCA), non-negative matrix factorization (NMF), discriminant analysis (DA), partial least squares (PLS), multivariate curve resolution (MCR), and maximum autocorrelation factors (MAF)[68–70]. These methods in general serve to identify statistically significant variances in the datasets that can provide information on chemical variations of the material or materials under analysis. Principal component analysis (PCA) is the most widely used MVA technique. The PCA method identifies ‘principal components’ that are combinations of secondary ion signals and represent large variances within a multi-dimensional dataset. Each sample or pixel is assigned a ‘score’ that reflects the significance or presence of each principal component in the dataset. Analysis of the different scores across

a set of samples can be used to determine chemical differences within a dataset. For example, Urquhart et al. performed ToF-SIMS studies on a polymer microarray containing 576 acrylate-based polymers. PCA analysis enabled the authors to easily identify polymers that had a surface enrichment of non-fluorinated monomers.[71] More information on multi-variate analysis techniques can be found in the literature.[68–70]

2.5 Additional features and advanced techniques

Several techniques have been developed that either enhance the capabilities of ToF-SIMS or combine ToF-SIMS with other surface analysis techniques. In 2016, Fisher et al. reported ToF-SIMS with tandem mass spectrometry (MS/MS) capabilities.[72] Tandem mass spectrometry involves two stages of mass spectrometry analysis[73] and is particularly useful for the analysis of large or complex molecular ions, common in biomaterials.[74] The technique involves acquiring a full ToF-SIMS spectrum and selecting desired secondary ion peaks for further analysis. Fragments within a *1 m/z* window are sent to a collision-induced dissociation (CID) cell which further fragments the ions and produces a secondary mass spectrum. This technique provides useful additional information to aid in the identification and analysis of secondary ions with no need of a reference, and the technique is also compatible with imaging and depth profiling. As an example, Fisher et al. analyzed the cross-section of a zebra finch brain and performed tandem mass spectrometry analysis on the *m*/*z* 255 fragment. This resulted in an MS/MS spectra that enabled the authors to identify the peak as corresponding to palmitic acid[72]. Tandem mass spectrometry capabilities are now available in some commercial ToF-SIMS systems.

The combination of ToF-SIMS with atomic force microscopy (AFM) enables characterization of both chemical and structural features of a material. Conventional ToF-SIMS analysis does not account for or detect topographical variations of a surface, and different organic materials can sputter at different rates[75]. This can lead to artifacts and uncertainty in the interpretation of mass spectrometry images or depth-profiling analyses.[76] The combination of ToF-SIMS with AFM can overcome these challenges and also provide additional advantages, such as the ability to resolve features with higher resolution than by ToF-SIMS alone[77] and avoiding changes in surface chemistry and structure when transferring between instruments.[76] Bernard et al. used a combination of AFM and ToF-SIMS to analyze a bulk heterojunction organic photovoltaic film. Through AFM height and phase analysis combined with ToF-SIMS analysis, they were able to acquire chemical information on domains smaller than the resolution capabilities of ToF-SIMS.[77] In a recent study, Miyagi et al. utilized a combined ToF-SIMS and AFM instrument to analyze chemical and structural changes on the surface of a polymer blend film. They created a wedge crater in the polymer film to a maximum depth of 40 nm. Next, the film surface was analyzed before and after thermal

annealing to investigate changes in surface chemistry due to migration of polymer additives to the damaged surface. The authors analyzed the film by AFM after thermal annealing to quantify changes in the material topography. With this combination of techniques, the authors demonstrated that the surface chemistry of the material was able to "self-heal" due to migration of polymer additives to the damaged site but the surface topography did not change.[40]

Other examples of advanced ToF-SIMS capabilities include the combination of ToF-SIMS with a focused-ion beam (FIB) which can be useful in the analysis of hybrid materials[78], the combination of helium-ion microscopy with ToF-SIMS which can provide excellent spatial resolution along with chemical analysis by ToF-SIMS[79], the Storing Matter technique which can enhance the intensities in the higher-mass range compared with conventional ToF-SIMS[80], orthogonal SIMS which can produce improved sensitivities and mass resolving power[81], and the analysis of liquid samples by ToF-SIMS using liquid secondary ion mass spectrometry (liquid SIMS).[82]

Section 3: Analysis of Polymer Films and Coatings

3.1 Spectral Analysis

The spectral analysis mode can evaluate the composition and lateral uniformity of polymer coatings, as well as detect/quantify the density of functional groups on a polymer surface. Spectral analysis is a simple yet powerful approach for characterizing polymer coatings that are prepared by reactions on a surface, such as polymer brushes and plasma polymer films. Polymer brushes are frequently used to modify the chemistry of a substrate[83] and are prepared by grafting-to or grafting-from reactions. Spectral analysis can probe the structure of a brush by evaluating its composition at different etch depths,[84,85] which is useful for characterizing order in block copolymer brushes.[85] Surface spectral analysis can also be used to test for compositional homogeneity within a sample, and among samples, by mapping the surface composition. Such data can inform the development of grafting-to or grafting-from protocols. As an example, Schulz et al. grafted ultra-thin poly(N-isopropylacrylamide) (PNIPAAM) brushes from silicon substrates with surface-initiated atom transfer radical polymerization (SI-ATRP).[86] Spectral analysis confirmed that thin PNIPAAM brushes were successfully grown across the surface of each sample, and the chemical composition of the brushes was consistent for a range of activator/deactivator ($[Cu(II)]_0/[Cu(I)]_0$) ratios. Plasma polymerization is a common technique for preparing thin, mechanically robust films on a substrate. Spectral analysis can determine whether a plasma-polymerized coating has the same chemistry as one prepared from a commercially available polymer (i.e., a polymer that was synthesized in solution). As an example, Oran et al. showed that the chemistry of plasma-polymerized poly(allylamine) coatings depends

on the plasma conditions and is distinct from a commercial reference.[87] This was attributed to different extents of branching and crosslinking in each material.

Spectral analysis can also detect functional groups at the surface of a polymer film and quantify their coverage using a calibration curve. Hadjesfandiari et al. used spectral analysis to inform the design of antimicrobial coatings for platelet storage bags. Specifically, they detected a low concentration of antimicrobial peptides (AMPs) that were conjugated to a polymer coating and further demonstrated that the AMP coverage was uniform across the surface.[88] Kim et al. showed that spectral analysis can quantify the surface density of amines in plasma-polymerized ethylenediamine films,[89,90] which is tunable through changes in plasma power. Their approach used a calibration curve that related secondary ion signals to amine densities that were determined by infrared (IR) and ultraviolet-visible (UV-vis) absorbance spectroscopies. As amines do not absorb UV-vis light and provide a weak signal in IR, these moieties were reacted with chemical tags (benzaldehydes) that provided a strong signal for each technique. Fragments of the same chemical tags were also detected in the TOF-SIMS measurements. The authors identified two secondary ion signals that were proportional to the surface amine density, as shown in Figure 5. This study demonstrated that ToF-SIMS could be used along with surface derivatization techniques to perform quantitative analysis of surface functionality. However, an independent method such as UV-vis, IR or XPS is required to calibrate the signal.

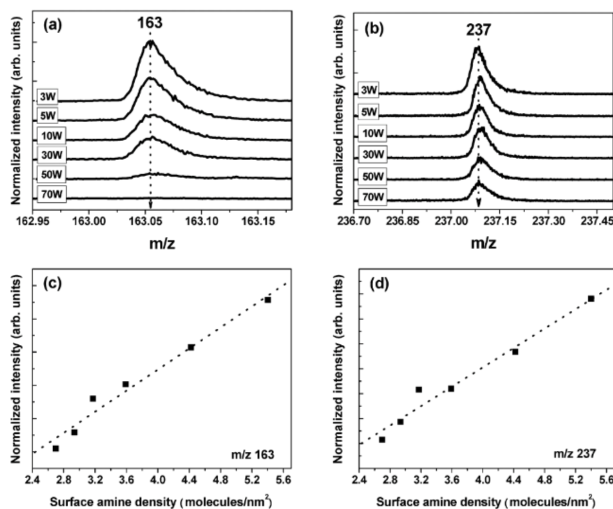

Figure 5. Normalized negative ToF-SIMS spectra of AMP-polymer conjugates as a function of plasma power. (a) *m/z* 163 after reaction with 4-nitrobenzaldehyde and (b) *m/z* 237 after reaction with pentafluorobenzaldehyde. Corresponding calibration curves are shown in (c) m/z 163 and (d) m/z 237. Reproduced with permission from Ref. [88].

3.2 Imaging

The ToF-SIMS imaging mode can map the chemistry of micropatterned polymer surfaces. As an example, the patterning of polystyrene by "breath figures" is well-documented in the literature.[91,92] This technique involves spreading a polystyrene solution on a surface under humid conditions, and as solvent evaporates, the surface cools and water condenses. The droplets of condensed water template the formation of a honeycomb structure, i.e., hexagonal arrays of micropores. Many studies have shown that this patterning process is highly effective when using polystyrene with polar end groups.[92] Yunus et al. and Galeotti et al. used ToF-SIMS imaging to examine the spatial distribution of polar end groups within the honeycomb structure.[93,94] These studies showed that the polar end groups were enriched within the microcavities, demonstrating that chemical patterns can be formed within the ordered topography (Figure 6a). Photolithography is another common approach for micropatterning of polymer films. Dubey et al. used a positive-tone photoresist to introduce chemical patterns in a coating of poly(ethylene glycol) that was derivatized with N-hydroxysuccinimide (NHS).[95] After development of the patterns, which produces alternating regions with and without the photoresist, the sample was immersed in a solution of 2-methoxyethylamine to convert the exposed NHS moieties to methoxy (MeO) groups. The remaining photoresist was then stripped to reveal a pattern of alternating NHS and MeO functional groups, where the NHS sites could be used to immobilize biomolecules while the MeO sites were passive. Aided by PCA, ToF-SIMS imaging could discriminate between areas with NHS versus MeO moieties and confirm the formation of chemical patterns. Additionally, these studies revealed a distinct chemistry at the border of the NHS and MeO patterns that was caused by residual photoresist. The authors noted that atomic force microscopy could not detect any topography associated with this residue, demonstrating the value of ToF-SIMS imaging for quality control in a lithographic process. Du et al. showed that UV exposure could trigger the polymerization of dopamine, providing a simple route to generate polydopamine (PD) micropatterns by photolithography.[96] PD is a near-universal adhesive that binds to metals, oxides, and polymers,[97] and patterns of PD could be used to anchor other species (such as nanoparticles) into regular arrays. The authors used ToF-SIMS imaging to confirm the formation of well-defined micropatterns, as shown by the CN^- intensity map in Figure 6b. Spectral analysis in negative ion mode showed a strong signal corresponding to a dopamine dimer, which confirmed that UV-triggered dopamine polymerization produces a similar PD structure as the common base-triggered dopamine polymerization.

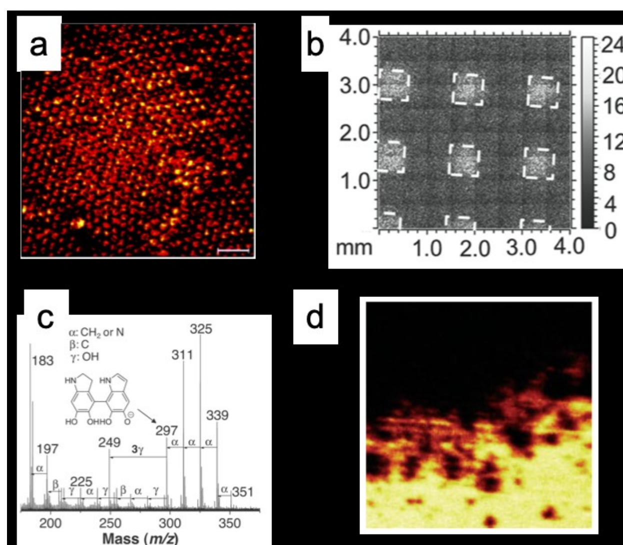

Figure 6. (a) ToF-SIMS image (CN^- intensity map) for honeycomb PS films prepared by breath figure patterning (scale bar = 10 μm). Reproduced with permission from Ref. [94]. (b) ToF-SIMS image (CN^- intensity map) of photopatterned polydopamine on a silicon wafer; and (c) ToF-SIMS spectrum acquired from polydopamine surface. Reproduced with permission from Ref. [96]. (d) ToF-SIMS image (F^- intensity map) of PVDF/PU interface. Reproduced with permission from Ref. [98].

ToF-SIMS imaging can also be used to examine a buried polymer/polymer interface. Hinder et al. used ultra-low-angle microtomy to expose the interface between a poly(vinylidene difluoride) (PVDF) film and an underlying polyurethane-based (PU) primer.[98] Both the PVDF and PU were commercial materials that included additives. Positive and negative ToF-SIMS ion maps revealed a heterogeneous interface with island-like structures that were caused by the topography of the PU primer. Measurements in negative ion mode could detect several identifiable fragments from each layer that reflected the complex commercial formulations: fragments from both aromatic and aliphatic monomers of the PU, the diisocyanate crosslinker in the PU, additives in PU, vinylidene difluoride in PVDF, and an acrylate copolymer additive in PVDF. More significantly, these data showed that the interface composition was distinct from that of the bulk PVDF or the bulk PU. Specifically, the interface was enriched in the acrylate copolymer additive. While the primary function of these additives was to improve the bulk mechanical, rheological and optical properties of PVDF, this study showed that interfacial excess provides a secondary benefit of enhancing adhesion to PU.

3.3 Depth Profiling

When reactions are used in post-deposition modifications of polymer films, the changes in chemistry are not always restricted to the near-surface region. Depth profiling can characterize the extent that the reaction front propagates into the film. Guo et al. showed that post-polymerization modification (PPM) of polymer brushes could lead to surface wrinkles with a tunable periodicity.[99] The PPM involved crosslinking the outer layer of poly(styrene-alt-maleic anhydride) brushes with cystamine under poor solvent conditions. When the modified brushes were immersed in a good solvent, anisotropy in the swelling (in-plane versus through-plane) produced a compressive stress that was relieved through wrinkling. The wavelength of the wrinkles was controlled by PPM time. ToF-SIMS depth profiling was used to detect the intensities of secondary ions from the brush backbone ($C_3H_3^+$), the cystamine crosslinker (H_3S^+), and the silicon substrate (Si^+) as a function of depth from the free surface. These data revealed that the penetration depth of cystamine into the brush increased with PPM time, following a linear relationship until conversion of the anhydride reached approximately 50%. The authors proposed that such kinetics are indicative of a PPM mechanism that involves the propagation of a cystamine front into the brush. Kim et al. compared the effectiveness of plasma-enhanced ion implantation and traditional plasma treatment for surface modification of poly(ethylene terephthalate) (PET) with CF_4.[100] Spectral analysis in positive ion mode detected a range of fluorine-containing fragments, including CF^+ and CF_3^+, as well as $C_8H_5O_3^+$ fragments from PET. By normalizing the different fluorine signals to that of $C_8H_5O_3^+$, the authors concluded that plasma-enhanced ion implantation introduces more fluorine at the surface than traditional plasma treatment methods, and these were consistent with XPS measurements of the surface. Depth profiling ToF-SIMS measurements showed that this trend persisted deeper into the film, leading to differences in the thickness of the modified layer. However, the authors did not consider the possibility that the different surface treatments could damage or affect the polymers differently, which could produce changes in the intensity of the $C_8H_5O_3^+$ reference signal as a function of depth. Rupper et al. developed functional plasma polymer films with a graded structure using CO_2/C_2H_4 discharges. The surface layer contained a high concentration of functional groups, including hydroxyl and carboxyl moieties, and the base layer was highly crosslinked to enhance chemical stability.[101] With depth profiling, the authors showed that a higher fraction of oxygen-containing fragments (such as C_2HO^-, C_3HO^-) were detected from the surface layer than the base layer. The transition from surface to bulk was sharp, with a steep decline in the oxygen-containing fragments past a depth of 1 – 2 nm.

Depth profiling can be used to probe diffusion of a small molecule penetrant in a thin polymer film. As an example, Bottoms et al. examined diffusion of sodium triflate in a polymeric photoresist,[102] where sodium triflate was employed as an inert analogue of a common catalyst (acid triflate). They prepared

bilayers with a base "feeder layer" containing sodium triflate and a top "diffusion layer" that initially contained no ions. The thicknesses of the base and top layers were approximately 400 nm and 600 nm, respectively, so the bilayer interface was at a depth of 600 nm from the free surface. When the bilayer was heated, the ions diffused across the interface. The authors tracked the F^- signal from triflate and, with the use of a calibration curve, were able to quantify the depth-dependent concentration (Figure 7). These depth profiles were then analyzed with Fick's second law to extract the diffusivity. The authors noted that the as-prepared bilayer interface was sharp, but the apparent resolution in the ToF-SIMS measurement was $\sigma \approx$ 20 nm. This loss of resolution is attributed to non-uniform etching, where the surface becomes increasingly rough with sputter time. A consequence of this behavior was that short-time diffusion (small diffusion lengths) could not be examined with this technique. However, long-time Fickian behavior was easily resolved for a range of photoresist formulations and process temperatures.

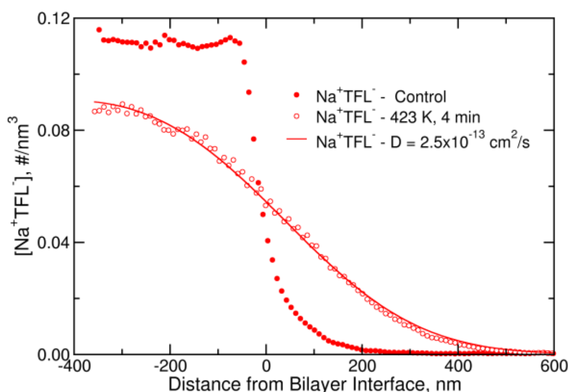

Figure 7. Depth profiling of sodium triflate in poly(hydroxystyrene-co-acrylic acid-co-styrene). In the as-prepared bilayer (control), the concentration of sodium triflate (Na^+TFl^-) in the feeder layer was 0.11 #/nm^3. After heating at 423 K for 4 min, sodium triflate diffused across the interface. The optimized diffusion model is shown by the red line. Adapted from Ref. [102].

Depth profiling in conjunction with imaging can map the three-dimensional composition of a polymer film, which is useful for characterizing multilayer structures and detecting interior defects. Mei et al. demonstrated that UV-initiated thiol-ene reactions could rapidly crosslink bottlebrush polymer films.[103] This approach took advantage of the polynorbornene backbone chemistry, which provided the alkene sites, along with thiol-terminated side chains or a multifunctional thiol additive. The crosslinked bottlebrush films were insoluble, so multiple layers with differing chemistry were prepared through sequential solution

casting and crosslinking steps. An example of a multilayer film is shown in Figure 8a, where depth profiling in conjunction with imaging confirms the formation of distinct alternating layers of PS and PMMA.[103] Note that depth profiling with ToF-SIMS can be extended beyond binary systems.[104,105] Ren et al. showed that spin-coated films of poly(bisphenol A decane ether) (BA-C10) exhibit a complex topography in optical microscopy, including droplets and striations, that depends on the type of solvent used for casting.[106] The authors examined the structure of these topographic features using a combination of depth profiling and imaging. They tracked signals unique to the polymer ($C_9H_{11}O^+$, $C_3H_5^+$) and the silicon substrate ($SiOH^+$) and found that the substrate signal rose faster in the center of the droplets than in the surrounding valleys. This observation, along with cross-sectional views of the 3D image, suggested that the droplets were hollow inside (Figure 8b-c).

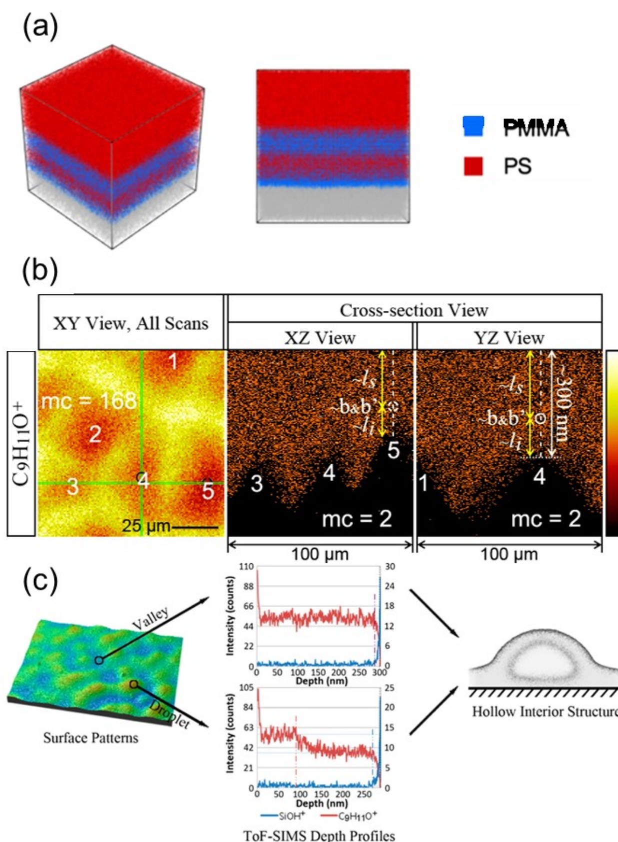

Figure 8. ToF-SIMS depth profiling analysis of a polymer multilayer coating (a) and spin-cast polymer films (b and c). (a) False-color spectra for PS/PMMA multilayer coating reconstructed from ToF-SIMS depth profiles. Red, blue, and gray colors indicate PS, PMMA, and the silicon substrate, respectively Reproduced with permission from Ref. [103]. (b) and (c) Spin-coated BA-C10 films with THF as the solvent: (b) in-plane and through-plane view of ion counts from the polymer; (c) from left to right: surface

topography by optical profilometry; Depth profiles reconstructed retrospectively from the valleys and droplet; a schematic of the inferred hollow droplet structure. Reproduced with permission from Ref. [106] .

Section 4: Polymer Blends

Section 4.1: Spectral Analysis

Spectral analysis can quantify the surface composition of polymer blends. This approach requires ToF-SIMS signals that are unique to each polymer, which is often aided MVA techniques such as PCA.[107] The signals are then converted to composition by using a calibration curve, or in cases where matrix effects are negligible, the relative signals are directly proportional to the blend composition. A secondary measurement such as XPS is used to establish the relations between ToF-SIMS signal and composition, rather than known proportions of each polymer in the blend, as the surface is usually enriched by the lowest energy constituent(s).[50] As an example, Cossement et al. used spectral analysis to quantify the surface composition of PMMA/poly(L-lactide) (PLA) blends for a range of blend compositions.[107] The ToF-SIMS spectra from PMMA and PLA have some similarities, as they are both hydrocarbons with ester-based repeat units. PCA analysis was used to identify the peaks that were characteristic of each polymer, such as $C_4H_5O_2^-$, $C_3H_3O^-$, and $C_8H_{13}O_2^-$ for PMMA and $C_3H_3O_2^-$, $C_3H_3O_3^-$ and $C_3H_5O_3^-$ for PLA, although some of the peaks could likely be identified through visual comparison with homopolymer reference spectra. The surfaces of several blends were then measured with ToF-SIMS spectral analysis as well as XPS. The authors used partial least squares regression to show a good correlation between the surface compositions by XPS and spectral analysis, where the latter was based on all the ToF-SIMS signals that were characteristic of PMMA and PLA. In another example, Dekeyser et al. examined the surface composition of a polymer bilayer that was prepared by spin coating poly(methyl methacrylate-co-methacrylic acid) on top of PS.[108] Pure PS and acrylic films were measured by spectral analysis, and the ToF-SIMS signals that are characteristic of each material were determined through comparison with published spectra for PS and PMMA. Spectral analysis of the bilayer showed that both polymers were present at the surface, demonstrating that the PS base layer was partially dissolved during spin casting of the acrylic overcoat (from chlorobenzene). The surface was also imaged by atomic force microscopy, revealing phase-separated domains that confirm the findings from ToF-SIMS measurements.

Section 4.2: Imaging

ToF-SIMS imaging can resolve phase separation in binary and multi-component polymer blends. MVA is often used for such studies: these methods can help to distinguish two (or more) polymers that share a common chemical motif, and also enhance the chemical contrast for samples with small domains, large variations in surface topography, and when the measurement is challenged by sample charging and degradation.[109–111] Trindade et al. examined thin film blends of two immiscible polyesters (20 μm thick).[109] The variables for the experiments were type of substrate (aluminum or zinc), blends with or without a pigment, and cured or uncured. The blends were provided by a commercial partner, so the exact chemistry was unknown, but the partner also provided control samples of the pure polyesters (both cured and uncured). Ultralow-angle microtomy was used to prepare cross-sections for imaging the through-film blend structure, with the aim of resolving both the bulk and interfacial regions. The authors acquired 28 data sets for 4 types of blend samples (6 patches per sample, each 500 μm x 500 μm) and 4 control samples. These data were processed by NMF. As shown in Figure 9a, the surfaces of two polyester control samples were distinguishable before curing but appeared identical after curing. The cross-sectional images of the blends show that polyester "2" is always concentrated at the top surface and is also enriched at the bottom surface when the formulation includes the pigment. The bulk layer in all coatings shows phase-separated structures, and the domain sizes were larger in blends with no pigment and on zinc substrates. Kono et al. examined immiscible blends of PS and poly(1,4-butadiene) (PB).[110] Spectral analysis was used to examine pure PS and PB reference samples for two different doses of the primary ion beam, revealing degradation. Signals that were characteristic of each material were readily identified by visual inspection of the spectra, with m/z = 41 for PB and m/z = 91 for PS (positive ion mode) selected for further analysis. As shown in Figure 9b, the image map for m/z = 41 shows speckle patterns rather than clearly defined domains. The authors explored two approaches to enhance the chemical contrast. First, they evaluated six MVA techniques and determined that PCA showed the highest chemical contrast, but the morphology was still difficult to resolve. Second, they stained the samples with OsO_4, which reacts with the double bonds on PB. Clear images were obtained from the O^- signal without using MVA for contrast enhancement. The authors speculated that in the absence of staining, MVA failed to produce a high-quality image because there was a large amount of PS in the PB-rich domain. Ravati et al. examined the phase-separated structures in ternary blends of polylactic acid (PLA), polybutylene succinate (PBS), and polycaprolactone (PCL). As these three polyesters have similar chemical structures, it is difficult to identify the phases through microscopy: common techniques to enhance contrast, like extraction of one polymer in a selective solvent, are not viable. The authors used PCA of pure polymers to identify signals that were unique to each constituent. As examples, m/z=69 ($C_5H_9^+$), m/z=101 ($C_4H_5O_3^+$) and m/z=56 ($C_3H_4O^+$) are characteristic of PLA, PBS and PCL, respectively. Figure 9c includes images from a binary PLA/PCL blend (left panel) and the ternary

PLA/PBS/PCL blend (middle panel), which are constructed by overlaying the $C_5H_9^+$ (blue), $C_3H_4O^+$ (green) and $C_4H_5O_3^+$ (red) signals. Both blends show macroscale phase separation, and PLA forms an interfacial wetting layer in the ternary system. The authors also tested whether MCR could identify the phases in the ternary blend; in contrast to PCA, this technique does not require prior knowledge of the constituents. Figure 9c shows the results of MCR analysis (right panel), shows the same interfacial wetting layer as determined through PCA.

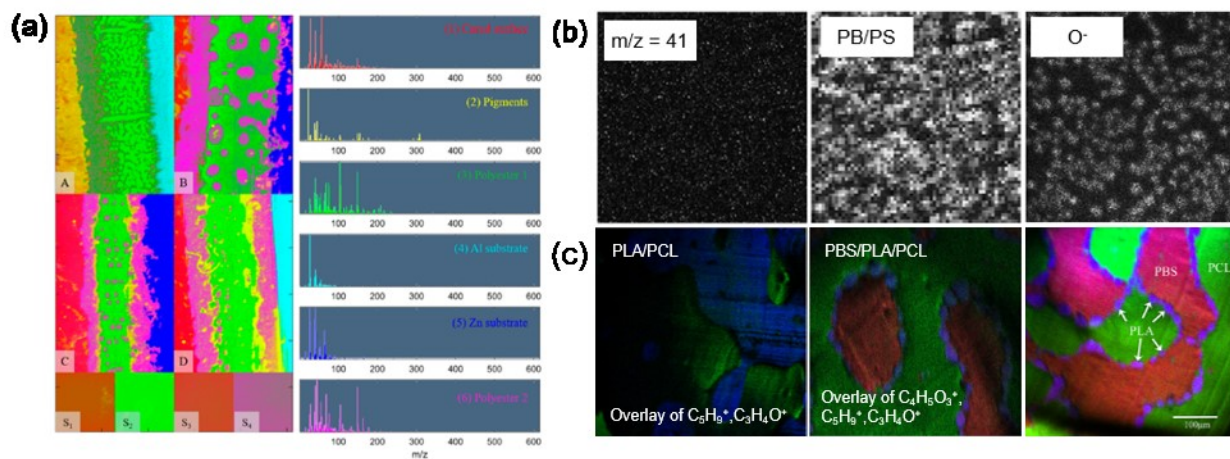

Figure 9: a) Morphology of binary polyester blends on Al and Zn substrates, with and without pigment, was identified by NMF analysis. The images to the left are overlays of all components indicated in the spectra on the right, where each component is assigned one color. Reproduced from Ref. [109] b) The left image is a map of m/z = 41, characteristic of PB. The middle image is the chemical contrast from PCA, effectively a ratio of PB to PS content. The right panel is the O^- signal from stained films. Adapted from Ref. [110] c) Morphology and binary and ternary polyester blends. The left and middle images, spanning 400 μm x 400 μm, are constructed from an overlay of the $C_5H_9^+$ (blue, PLA), $C_3H_4O^+$ (green, PCL) and $C_4H_5O_3^+$ (red, PBS) signals. These signals were identified through PCA. The right panel is based on MCR analysis, where blue, green, and red correspond with PLA, PCL, and PBS, respectively. Adapted from Ref. [112].

Section 4.3: Depth Profiling

In polymer blends, one constituent is typically enriched at surfaces and interfaces. ToF-SIMS depth profiling is a powerful approach to probe this enrichment,[58,113,114] and with appropriate calibration this technique can even quantify the excess. As an example, Mahoney et al. examined the through-film composition in blends of poly(L-lactic acid) (PLLA) and Pluronic surfactant, which is an ABA triblock copolymer based on poly(ethylene oxide) (PEO) end blocks and a poly(propylene oxide) midblock.[114] This

blend system is of interest for drug delivery implant systems, as PLLA is biodegradable, Pluronic can encapsulate the drug, and Pluronic is also thought to improve biocompatibility by accumulating at the surface of the device. Spectral analysis of pure Pluronic and PLLA films was used to identify peaks that are characteristic of each material, and in the positive ion spectra, the signals selected for depth profiling were m/z = 59 for Pluronic and m/z = 56 or 128 for PLLA. The blend films (700 nm thick) were then depth profiled to examine the distribution of Pluronic throughout the thickness. The depth profiles showed a clear enrichment of Pluronic at the free surface, followed by a narrow depletion region immediately beneath the surface, a wide bulk region of uniform composition, and a modest enrichment of Pluronic at the substrate. Stein, Verduzco and coworkers used depth profiling to examine surface enrichment in architecturally complex polymer blends, where the major component is a linear commodity polymer, and the minor component is a bottlebrush polymer additive.[40,41,58] In one such study, they examined an athermal blend of linear polystyrene with bottlebrush polystyrene additive, where the additive was partially deuterated to provide an easily identifiable signal ($^2H^+$) in ToF-SIMS spectra.[58] The architectural variables for the study were degree of polymerization (DP) of the linear polystyrene (N_m), DP of the bottlebrush side chains (N_{sc}), and DP of the bottlebrush backbone (N_b). Thin films (ca. 300 nm) were cast from chlorobenzene, thermally annealed to equilibrate the structure, and depth profiled with ToF-SIMS. The $^2H^+$ intensity was normalized by C^+ and converted to bottlebrush composition (mass fraction φ) with a calibration curve (Figure 10a). We note that the ratio of $^2H^+/C^+$ intensities was linear with actual deuterium content, which might indicate that matrix effects are negligible in polymer blends where the only difference between constituents is an isotopic label. Furthermore, if a linear relationship is either demonstrated or assumed for such blends, then the signal can be converted to composition without a calibration curve: A scaling factor that converts signal to composition can be determined using the known overall blend composition and sample thickness. The depth profiles revealed conditions that drove depletion or enrichment of the bottlebrush at the surfaces, as well as cases where the surface composition matched that of the bulk (Figure 10b-c). These results showed qualitative agreement with simulations based on self-consistent field theory that incorporated a weak enthalpic preference for linear PS at the air surface.

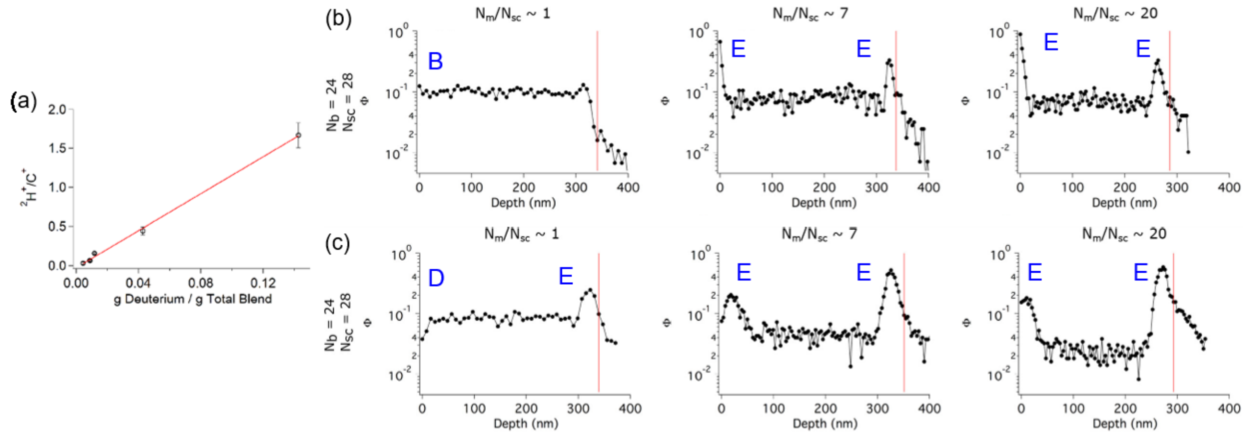

Figure 10. ToF-SIMS depth profiling of linear polystyrene with 10 wt% bottlebrush polystyrene additives. (a) Calibration curve shows that normalized deuterium counts are directly proportional to mass fraction of bottlebrush additive. (b) Depth profiling of as-cast films. (c) Depth profiling of thermally equilibrated films. B = surface composition matches bulk composition; E = bottlebrush enrichment; D = bottlebrush depletion. Adapted from Ref. [58].

Section 5: Polymer composites

Section 5.1: Spectral Analysis

Polymer composites are composed of a filler incorporated into a polymer matrix.[115,116] Each filler type has distinct surface properties that are not always compatible with the polymer matrix, leading to bonding issues between the filler and matrix. This is especially relevant when using natural fibers, as these exhibit polar surface characteristics that are incompatible with commodity polyolefins such as polypropylene.[117,118] Consequently, the surfaces of natural fibers are often modified through chemical treatments to enhance interactions with the matrix. ToF-SIMS can detect these modifications and discriminate between the near-surface and bulk composition, where the former is critical for applications in composites. As an example, Zafeiropoulos et al. examined the pre-treatment of flax fiber surfaces by reactions with acetic anhydride (acetylation) and stearic acid (esterification) to increase the hydrophobicity.[117] Spectral analysis was employed to confirm successful acetylation through detection of CH_3COO^- ions and successful stearic acid incorporation through detection of $C_{17}H_{35}CO_2H_2^+$ and $C_{17}H_{35}C{=}O^+$ ions. ToF-SIMS is also able to determine the efficiency of the treatments. Furthermore, the relative ion intensities changed when measured at different positions along the treated fibers, demonstrating that the pre-treatments produced heterogeneous surfaces. Freire et al. showed similar results for the esterification of cellulose fibers by fatty acids:[118] by

mapping $CH_3(CH_2)_nCO^+$ ion counts across the surface, they determined that the treatment was successful but highly heterogeneous.

In the manufacturing of high-performance composites, individual parts are molded and then assembled into a final structure. The molds are coated with release agents such as fluorine- or silicon-containing films. Residue from these films can reduce the surface energy of the part,[119] which influences how two part bond together.[120,121] Bénard et al. demonstrated that polyamide or polyester peel plies can be used to alter the surface chemistry of carbon/epoxy and glass/epoxy composites to improve bonding.[122,123] The peel-ply layer was impregnated into the composite during the curing step and then removed prior to use of the part. ToF-SIMS analysis of the composite/peel ply contact area revealed that polyamide peel plies introduced a variety of polar groups at the surface, as evidenced by the increase of nitrogenous containing species (NH, CNO, $C_6H_{12}NO$), while polyester peel plies resulted in more non-polar carbonated groups (CH_3O, C_3H_7O, Phthalate). Another approach to alter the surface chemistry of the individual parts is post-cure processing. Gilbert et al. modified the surfaces of carbon fiber and E-glass epoxy resin composites with an Accelerated Thermo-molecular adhesion Process (ATmaP).[124] ATmaP atomizes N-methylpyrrolidone liquid and then vaporizes it, resulting in a surface reaction that increases the concentration of polar functional groups and also decreases contamination. ToF-SIMS analysis of treated and untreated samples detected approximately 20 distinct mass fragments (positive ion mode). Given the complexity of the spectra, PCA was used to differentiate between sample types and treatments. The authors found that the key differences between sample types were $C_xH_yN^+$ ions from E-glass and Si^+, $Si_2C_5H_{15}O^+$ and $Si_3C_5H_{15}O_3^+$ ions from carbon fiber, where these silicon-containing fragments were due to surface contamination by the release agents. Furthermore, ATmaP-treated samples showed high counts of $C_2H_3O^+$ and $C_5H_7^+$ ions, where $C_2H_3O^+$ was representative of oxidation while $C_5H_7^+$ was a consequence of chain scission. Spectral analysis coupled with PCA has also been used to study surface oxidation of polymer composites in extreme environments, including low earth orbit conditions and high temperatures with intense ultraviolet light.[115,116]

Section 5.2: Imaging

In manufacturing of composites, the spatial distribution of fillers will impact mechanical properties. Karar and Gupta utilized ToF-SIMS to image the lateral distribution and cluster size of carbon nanotubes (CNTs) in polyurethane (PU) films, and then correlated this information to the strength of the composite.[125] The ToF-SIMS spectrum of CNTs shows a variety of hydrocarbon peaks (such as $C_6H_5^+$, $C_4H_7^+$) that are distinct from those of PU, as well as a peak from residual iron catalyst (Fe^+). Therefore, imaging can map the CNT

location within the PU matrix. As seen in Figure 11a, small spherical clusters were observed with 1 wt% loading of CNTs, while larger, asymmetric clusters were observed at a loading of 5 wt%. The tensile strength was highest for 1 wt% loading.

Electronic properties are also influenced by clustering of fillers. For example, flexible electrodes based on graphene typically require a polymeric binder, and when the binder is non-conductive, the graphene must be well-dispersed to achieve high conductivity.[126,127] Brennan et al. used ToF-SIMS imaging to examine the dispersion of graphene in a conductive poly(3,4-ethylenedioxythiophene)-poly(styrenesulfonate) (PEDOT-PSS) binder, and in a non-conductive PMMA-based (MT46) binder.[128] ToF-SIMS could detect carbonaceous fragments from graphene, but the yield was low due to high bond strengths and low ionization potentials. Instead, these authors proposed that contaminant species in graphene, specifically sodium (Na^+), could be used to map its distribution. To test this idea, the authors blended two different graphene types, Carbon A and Carbon B, with both MT46 and PEDOT-PSS binders. Samples were prepared on an Aluminum foil. As shown in Figure 11b, a uniform Na^+ signal was detected from samples with Carbon A (and either binder), with little Al^+ signal. This is indicative of well-dispersed graphene. However, a heterogeneous Na^+ signal was detected from samples with Carbon B, and a strong Al^+ signal was detected in multiple patches. These maps are consistent with clumping of the graphene filler: the polymeric binders sputter more readily than graphene, exposing the foil in areas that are free of graphene. The authors also noted that reference spectra from pure PEDOT:PSS included Na^+, Al^+ and other ions, but these signals were much weaker than those produced by graphene or aluminum foil.

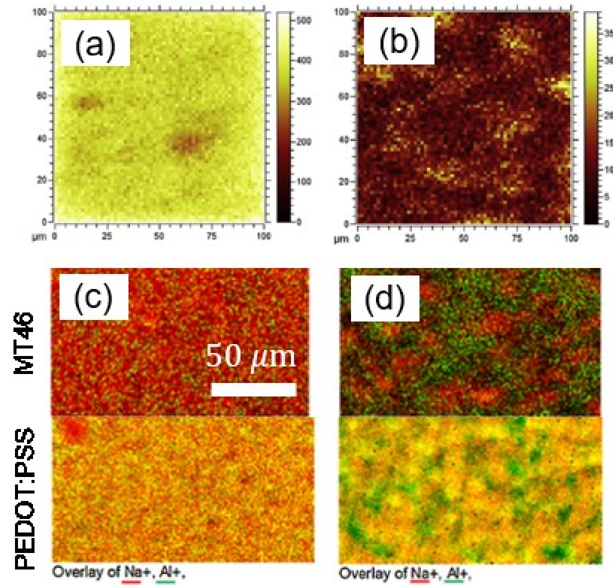

Figure 11. ToF-SIMS images showing the location and size of CNT clusters in a PU matrix, for a) 1 wt% CNT loading ($C_3H_5^+$) and b) 5% CNT loading ($C_2H_5^+$). Adapted from Ref. [125]. ToF-SIMS images showing graphene through sodium contaminant (Na^+) and the Aluminum substrate (Al^+), for c) Carbon A and d) Carbon B. Adapted from Ref [128] .

Section 5.3: Depth Profiling

In the electronics industry, polymer composites are widely used as an electrically conductive adhesive (ECA). Compared to lead based solders, they are more environmentally friendly, easier to produce, and processed at lower temperatures.[129] One drawback comes from the inherently lower conductivity resulting from the oxidation of the filler metal, specifically silver, during the curing process.[130] Yang et al. proposed a novel method to combat this oxidation by covering the exposed silver with treated silver iodide nanoislands, which are conductive and can also resist further oxidation.[129] Spectral analysis was used to determine the overall change in silver oxidation by monitoring the sum of Ag_2OH^+ and Ag_2O^+ over the silver base peak Ag^+. Since the oxidized signal comes from the base silver layer, and not the nanoislands, its detectability was controlled by the nanoisland coverage. As seen in Figure 12a, bare silver was further oxidized after curing. Silver with sparse to moderate coverage of the nanoislands experienced a decrease in the total oxidation after curing (Conditions 1 and 2), while an increase in oxidation was observed with a fully iodinated surface (Condition 3). Depth profiling was performed with the fully iodinated samples, both before and after curing, as shown in Figure 12b. A strong signal from silver hyperiodite ions ($AgIO^-$),

indicative of high oxygen incorporation in the nanoislands, was observed near the surface. Curing increased the amount of $AgIO^-$ in the near-surface region but had little impact deeper into the layer.

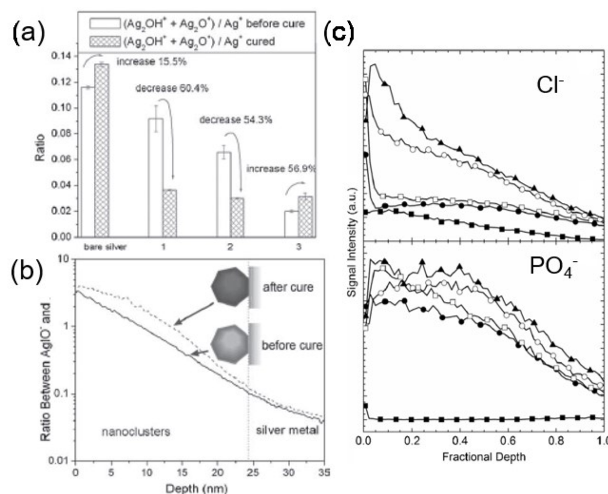

Figure 12: ToF-SIMS results demonstrating the reduction of silver oxidation due to the iodination process. a) comparison of bare silver to three different iodination treatment levels. b) ToF-SIMS depth profile of condition 3, which is the highest coverage of nanoclusters. Reproduced from Ref. [129]. c) Depth profiling of PPy/silk fibroin composites (12-20 µm thick) from a non-actuated film (solid squares), a cured film (open squares), and films after first reduction (solid circle), second reduction (open circle), and second oxidation (solid triangle). Reproduced from Ref. [131].

Conducting polymers can be used in actuation, but as these materials are often brittle, fillers are often used to improve the mechanical properties. As an example, Bradshaw et al. designed actuators based on interpenetrating networks of polypyrrole (PPy) and silk fibroin,[131] a system of potential viability for *in vivo* applications. They used ToF-SIMS depth profiling to examine changes in both dopant and ion concentration after actuation in phosphate buffered saline (which contains both phosphate and chloride ions). There was little change in the dopant concentration after multiple oxidation and reduction cycles. However, the ion concentration was changed after an initial cure phase that applies a large potential over a long time, and further changed through multiple actuation cycles. After curing, the authors showed an increase in the intensity of both phosphate (reflected by PO_3^- and PO_2^- fragments) and chloride (Cl^-). The chloride ions continued to build up after multiple actuation cycles while phosphate concentration was stagnant. These trends explain characteristics of the actuation performance: The buildup of anions inhibits anion movement, which explains why a large deflection during the initial cure is not repeated in subsequent

cycles. The buildup of chloride ions, which reflects an imbalance in the flow rates in and out of the film, could explain why expansion during oxidation is faster than relaxation during reduction.

Section 6: Analysis of Electronic Materials and Devices

6.1 Spectral Analysis

The solid-electrolyte-interphase (SEI) layer influences the safety, cycling stability, power output, and capacity of non-aqueous batteries, including lithium-ion batteries. The SEI layer is formed by the decomposition of electrolyte on the surface of the negative electrode and includes inorganic lithium salts, lithium carbonates, semi-carbonates, and polymers.[132] Electrolyte additives that react at the electrode surface have been used to improve the properties of the SEI layer. These reactive additives coat the negative electrode and can prevent or reduce side-reactions with the electrolyte but are not effective at elevated temperatures (above 50 °C). Okumura et al. proposed dimethallyl carbonate (DMAC) as an electrolyte additive to improve stability at elevated temperatures. They hypothesized that the multiple reactive functionalities of DMAC could provide improved stability in the resulting SEI film, even at elevated temperatures, due to the higher film crosslink density. They added DMAC to an electrolyte of 1 M $LiPF_6$ in a 1:2:2 blend of ethylene carbonate, dimethyl carbonate, and ethyl methyl carbonate and used a combination of X-ray photoelectron spectroscopy (XPS) and ToF-SIMS to analyze the SEI layer. Elemental depth profiles produced by XPS showed that a thicker SEI layer was formed when a higher weight fraction of DMAC was added to the electrolyte, and XPS also revealed a higher content of lithium alkyl carbonate in the SEI. ToF-SIMS provided additional insights into the molecular constituents in the SEI layer. Through analysis of both the positive and negative spectra, the authors were able to identify various fragments, including lithium alkyl carbonates, aliphatic hydrocarbons, and fragments produced from the decomposition of $LiPF_6$ or of the binder polyvinylidene difluoride (PVDF). By tracking the intensities of specific fragments as a function of DMAC content, they confirmed that the intensities of lithium alkyl carbonate-derived fragments (C_3O^- and $C_2H_3O_3^-$) and aliphatic-derived fragments ($C_6H_{11}^+$ and $C_5H_9^+$) increased while those derived from PVDF ($C_3F_4H_2^+$ and $C_3F_5H_2^+$) decreased or remained constant as the amount of DMAC additives increased. The authors concluded that the DMAC was incorporated into the SEI layer, and the thickness and coverage of the SEI layer increased with greater amounts of DMAC additives. The authors also found that the reversible capacity at elevated temperatures improved significantly when DMAC was used as an additive. The study demonstrates that additives such as DMAC can improve the stability of lithium-ion batteries at elevated temperatures and is an example of how ToF-

SIMS can be used in combination with other techniques, such as XPS, to gain detailed chemical insight into interfaces between hybrid materials.[133]

In another example where ToF-SIMS was used to examine composites relevant to energy storage, Konarov et al. investigated a composite of sulfur (S), dehydrogenated polyacrylonitrile (DPAN), and reduced graphene oxide (rGO) as a cathode material for an Li-S battery.[134] S is non-conductive, and both DPAN and rGO were added to provide electronic conductivity. Prior studies had established that S forms a covalent bond with DPAN, and Konarov et al. were interested in understanding how the binding between S and DPAN potentially changed during electrochemical cycling. The researchers used ToF-SIMS to track the binding between S and DPAN by analyzing the intensity of the CS^+ fragment, which reflected a C-S bond. Their electrochemical measurements suggested that polysulfides did not form during cycling, and ToF-SIMS revealed that the C-S bond was maintained in both the charged and discharged states and after 100 charge-discharge cycles (Figure 13). Their composite electrodes were able to maintain greater than 90 % of the initial capacity after 100 charge-discharge cycles. This study presented the first direct observation of C-S bonds in lithium-sulfur batteries.

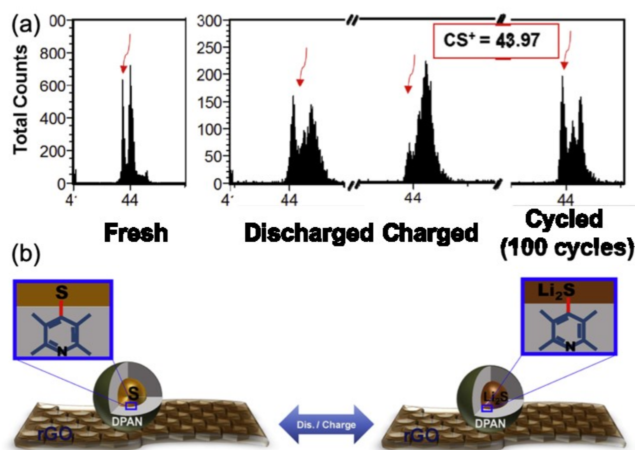

Figure 13. (a) ToF-SIMS spectra for S/DPAN composites (top) and (b) schematic for covalent binding between S and DPAN (bottom). The spectra show that the CS^+ ion fragment can be detected for freshly prepared electrodes and for both charged and discharged electrodes. Reproduced with permission from Ref. [134]. Copyright Elsevier.

6.2 Imaging

ToF-SIMS provides excellent sensitivity and can be used to identify multiple contaminants or low-concentration species in a single experiment. Kettle et al. demonstrated this in a study of the degradation processes in polymer bulk heterojunction (BHJ) OPVs. BHJ OPVs are multilayer organic devices that are typically sandwiched between metallic electrodes. They can be fabricated with either the anode or cathode on top, and these are referred to as normal or inverted configurations[135]. Kettle et al. compared the relative stabilities of devices with these different configurations and use a combination of XPS and ToF-SIMS to analyze chemical changes in the devices. Using the XPS, they were able to deduce active layer degradation mechanisms, which included chain scission, oxidation, and loss of side chains for the donor conjugated polymer and breakage of fullerenes and loss of molecular shape. They were also interested in studying the migration of metallic ions from the bottom electrode through the devices, but XPS provided insufficient sensitivity. However, the authors were able to observe In and/or Sn ions in some of the devices using ToF-SIMS. The bottom substrate for both types of devices was an indium-tin-oxide (ITO)-coated glass, and the presence of In or Sn on the surface of the devices would indicate that metallic ions migrated through the charge transport layers and the active layers to the top of the device. Prior studies have reported that ion migration is possible when the ITO surface is exposed to the conductive polymer PEDOT:PSS, which can etch ions from the surface of the ITO.[136,137] In the study by Kettle et al., the non-inverted device structure included a PEDOT:PSS film on top of the ITO-glass substrate. ToF-SIMS measurements detected both In and Sn ions on the surface of the active layer for the non-inverted devices only, and an ion image showing the distribution of $^{115}In^{+}$ is shown in Figure 14. While the authors were unable to determine a concentration of In or Sn on the top surface based on this analysis, the authors concluded that the migration of these ions contributed to the more rapid degradation of non-inverted devices.[138]

ToF-SIMS can also be used to analyze the distribution of Li^{+} ions in electrode materials for lithium-ion batteries. Fedorkova et al. compared $LiFePO_4$ electrodes containing either polypyrrole (PPy) or a blend of PPy and polyethylene glycol (PEG) as binder materials. While prior work had shown that PEG improves mechanical properties, the effect on Li^{+} ion distribution was unclear. Using ToF-SIMS, Fedorkova et al. produced ion images that showed the distribution of Li^{+} ions in the electrodes. Their analysis found that Li^{+} was uniformly distributed in the electrodes containing PEG, but they were unable to detect Li^{+} in the PPy electrodes without PEGs. This indicated that PEG improved the solubility of Li^{+} in the composite electrode. The authors also found that the electrodes with PEG exhibited higher electronic and ionic conductivities compared with those with only PPy.[139]

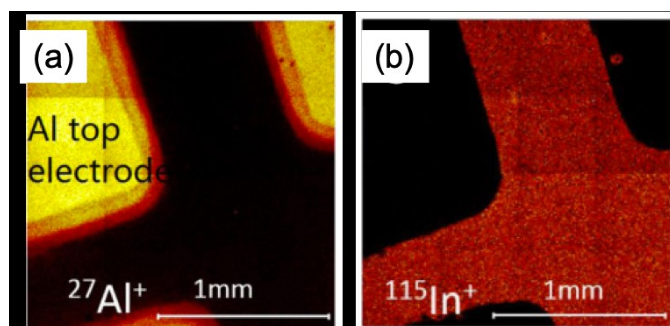

Figure 14. ToF-SIMS images show the ion distribution of (a)$^{27}Al^{+}$ and (b)$^{115}In^{+}$ on the surface of a non-inverted cell aged in air for 300 h. The images show the location of the Al top electrode and In^{+} impurities in the BHJ OPV that migrated from the bottom electrode. Reproduced with permission from Kettle et al.[138].

6.3 Depth Profiling

Bulk heterojunction (BHJ) organic photovoltaic (OPV) devices are multilayer organic devices. They generally include an active layer that is a blend of two organic semiconductors (typically a conjugated polymer as the donor and fullerene as the acceptor), charge transport layers, and electrodes. ToF-SIMS depth profiling studies have been conducted to determine interfacial widths, characterize compositional variations between and within layers, and study the dependence of secondary ion yield and depth resolution on the ion beam used for sputtering[140–144]. Mouhib et al. performed depth profiling studies on polymer/fullerene BHJ OPVs and found an apparent interfacial width in the range of 8 – 14 nm when sputtering with an argon cluster (Ar_{1700}^{+}) beam, but the apparent width of the interface at the bottom of the film with ITO was significantly larger (20 nm), indicating a buildup of roughness during depth profiling. They also observed much larger apparent interfacial widths when depth profiling with Cs^{+}. The authors of this study also concluded that it was important to use an energy of 10 keV or lower for the Ar_{1700}^{+}, which corresponds to approximately 6 eV per Ar atom[141]. Other studies have similarly investigated different ion sources for depth profiling and the dependence of beam energy on the sputtering process and reached similar conclusions[140,142,143]. Surana et al. investigated matrix effects in the depth profiling of polymer/fullerene OPVs both within each layer and at interfaces. They studied active layers comprised of C_{60} fullerene derivative phenyl-C_{61}-butyric acid methyl ester ($PC_{60}BM$) and different conjugated polymers, and systematically varied the mass fractions of $PC_{60}BM$ in the active layer. They observed a non-linear relationship in the negative fullerene ion yield for all active layer blends studied, as shown in Figure 15a. This demonstrates that quantification of the depth-dependent composition of these blends cannot be performed by assuming a linear relationship between secondary ion yield and composition. They also

observed a strong enhancement in negative fullerene ion intensity at the bottom interface on substrates with TiO_2, which they attributed to electron transfer between TiO_2 and PCBM.

Vertical stratification in organic electronic devices such as bulk heterojunction (BHJ) photovoltaics or organic light emitting diodes can improve performance[145,146], but controlling vertical stratification is not straightforward and may require tailoring the surface energies of the substrates and/or varying processing conditions.[147] Sun et al. investigated sequential, layer-by-layer (LBL) deposition of the donor and acceptor in the active layer as a method to control vertical stratification in the active layer.[148] Using ToF-SIMS depth profiling studies, they compared the vertical distribution of donor and acceptor in LBL deposited devices and conventional devices prepared by depositing a solution blend of donor and acceptor. The intensity of F^- as a function of depth reflected the relative composition of the donor polymer J71, and they observed significantly stronger vertical stratification in LBL-deposited devices. They demonstrated a 10% enhancement in power conversion efficiency for devices deposited by LBL and concluded that LBL deposition was a much simpler method for controlling the vertical distribution of donor and acceptor compared with alternative approaches.[148] Vertical stratification can also be beneficial to organic light-emitting diodes (OLEDs). Using ToF-SIMS, Murat et al. studied vertical segregation in inverted OLEDs consisting of a co-deposited layer of polyethylenimine ethoxylated (PEIE) and 1,3,5-tris(N-phenylbenzimidazol62-yl)benzene (TPBi) as the electron transport layer. They found that they could produce devices with similar performances whether these materials were co-deposited or deposited sequentially. ToF-SIMS depth profiling of $C_6H_5^+$ and $C_2H_4N^+$ ions, corresponding to TPBi and PEIE, respectively, demonstrated the PEIE spontaneously segregated to the bottom substrate. This was attributed to the higher surface energy of PEIE and a strong interaction with the underlying ZnO substrate.[149] In another study, Cao et al. studied the effects of interface layers on vertical stratification in BHJ OPVs. They showed that the deposition of a conjugated polymer with a lower surface energy than PEDOT:PSS affected the vertical distribution of donor polymer and $PC_{71}BM$ acceptor in the active layer. Specifically, the interface layer drove the donor preferentially towards the cathode, and the effect was most significant for low surface-energy polymers. This change in vertical distribution was also correlated with the device power conversion efficiency.[150]

The combination of depth profiling and imaging in ToF-SIMS provides a powerful tool for analyzing the chemistry and structure of buried interfaces in devices for energy conversion and storage. For example, hybrid solar cells are comprised of a bilayer of a conductive polymeric film and doped silicon, and the morphology and chemistry at the hybrid interface can influence the power conversion efficiency. While prior studies had investigated the effects of a thin native oxide layer on the power conversion efficiencies (PCEs) of hybrid solar cells[151], Thomas et al. were interested in understanding the effect of an

oxide layer on morphology of the polymer film. They analyzed a hybrid solar cell comprised of the p-type conducting polymer poly(3,4-ethylene-dioxythiophene):polystyrenesulfonate (PEDOT:PSS) on an n-type Si substrate. They performed ToF-SIMS depth profiling analyses using an Ar_{1000}^{+} sputtering beam to etch through the PEDOT:PSS film and analyze the interface between PEDOT:PSS and the Si substrate. Depending on the surface treatment of the underlying substrate, they observed either a smooth interface (for Si-H surfaces) or micropores (for substrates with an oxide layer). The researchers further demonstrated that the formation of the micropores depended on the oxide layer thickness and that thicker oxide layers produced larger micropore defects.[152]

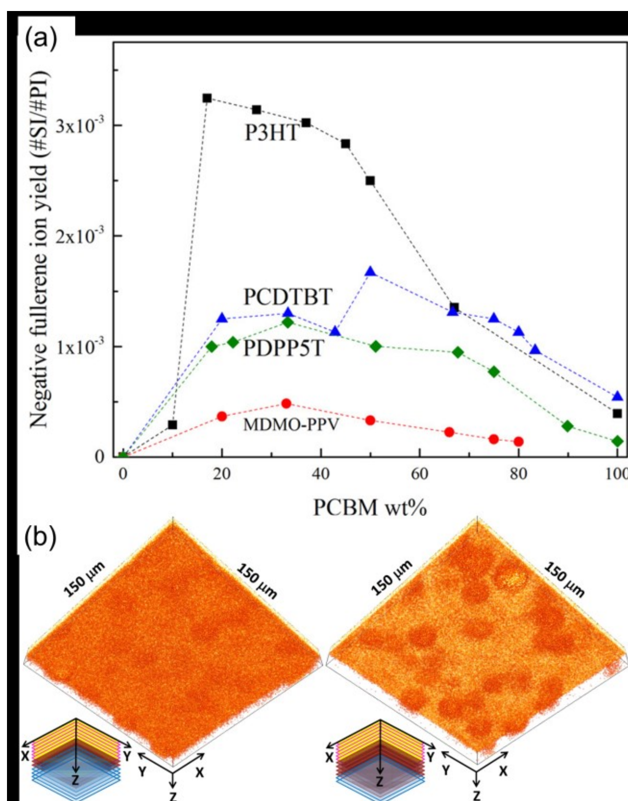

Figure 15. ToF-SIMS analyses of bulk heterounction OPVs. a) Negative fullerene ion yield measured in polymer:PCBM OPV active layers as a function of PCBM wt. % and for different conjugated polymer donors. All blends exhibit a non-linear dependence of the negative fullerene ion intensity with fullerene wt%. Reproduced with permission from Surana et al. Ref. [144] b) Bottom perspective TOF-SIMS images of $C_8H_7SO_3^-$ ions of PEDOT:PSS layers spin-coated on substrates with a (let) thin or (right) thick SiO_x layer. Large micropores are evident in the PEDOT:PSS layer on top of the thicker oxide layer. Reproduced with permission from Thomas et al. Ref. [152].

ToF-SIMS provides both excellent sensitivity and the ability to discriminate between different isotopes, and this enables semi-quantitative depth profiling analyses to understand degradation mechanisms in organic electronic devices. Norrman et al. used a combination of XPS and ToF-SIMS depth profiling studies, along with annealing of devices in controlled environments, to understand the effects of oxygen and water infiltration.[153] Using XPS, they were able to determine the amount of oxygen in both normal and inverted geometry devices, and they observed chemical changes in the active layer of the devices. Next, the authors exposed the devices to an environment of either dry $^{18}O_2$:N_2 or oxygen-free $H_2{}^{18}O$ atmosphere with the goal of separately understanding the contributions of water and oxygen to degradation of the devices. They found that XPS was not sufficiently sensitive to detect the additional oxygen uptake for this exposure step, but ToF-SIMS could easily distinguish between ^{16}O and ^{18}O and therefore quantify the amount of oxygen introduced in the controlled environments. By performing depth-profiling analyses of the devices exposed to different environments and calibrating the ToF-SIMS ion intensities using the XPS measurements, they were able to determine the ^{18}O uptake in different layers of the OPV devices and attribute them to either water or oxygen. These studies demonstrated that for devices kept in the dark, the highest concentration of ^{18}O was in the hole transport layer (PEDOT:PSS) and attributed to water in the environment. For devices that were illuminated, a higher concentration of ^{18}O was observed in the active layer and attributed to oxygen. The group also observed chemical and morphological changes for devices stored in the dark for 6 months, and ToF-SIMS was used to image morphological changes at the PEDOT:PSS interface. The authors concluded that morphological changes and degradation at the PEDOT:PSS-active layer interface were the primary failure mechanisms. This study demonstrates how ToF-SIMS can be combined with XPS to performed detailed, semi-quantitative studies of oxygen uptake and degradation.

Ghasemi et al. used ToF-SIMS to study kinetic and thermodynamic effects that influence the stability of BHJ OPVs that contain non-fullerene small molecular acceptors (NF-SMAs)[154]. The use of NF-SMAs in BHJ OPVs has led to devices with power conversion efficiencies approaching commercial viabililty,[155] but these devices have poor stabilities due to morphological changes in the active layers over time. To understand these morphological changes, Ghasemi et al. used ToF-SIMS to measure the diffusivities and Flory-Huggins χ-interaction parameter for 5 different SMAs blended with 5 different conjugated polymers. To measure diffusivities, they first prepared bilayers of the NF-SMAs and conjugated polymers. They were then thermally annealed, and ToF-SIMS depth profiles were performed to analyze the diffusion of the NF-SMA into the conjugated polymer layer. They obtained excellent fits to these depth profiles using a concentration-independent model based on a 1-D solution to Fick's 2nd Law, and the best fit of this model provided the NF-SMA diffusivity. Next, they used similar experiments to estimate the

equilibrium concentration of NS-SMA in the conjugated polymer host as an estimate of the bimodal, which represents the limit of solubility. The volume fraction of NF-SMA was determined by monitoring the intensities of F^-, Cl^-, or CN^- secondary ions, which were unique to the NF-SMA, and assuming that the NF-SMA and polymer had the same density (1.15 g cm^{-3}). Through these measurements, they were able to determine the temperature-dependent diffusivities, the activation energy for diffusion, and the χ-interaction parameter for each NF-SMA in each polymer host. These measurements revealed that the most incompatible polymer-NF-SMA blends produced the most stable devices. This is counterintuitive because it might be expected that the most incompatible blends would degrade due to morphological changes most quickly, but Ghasemi and coworkers showed that these blends also had the highest activation energy for diffusion and the lowest NF-SMA diffusivities. This work suggests a new approach to design thermally stable BHJ OPVs with NF-SMAs[154].

Outlook

ToF-SIMS is a powerful technique for mapping the chemistry of polymer surfaces. As described in the preceding sections, these measurements (often coupled with multivariate analysis) can resolve numerous effects that are important for fundamental polymer science, including functional groups that control the properties of a surface or filler, lateral phase separation and surface segregation in blends, the spatial distribution of fillers in composites, and the structure and composition of the SEI in lithium-ion batteries. We note that many of the examples discussed herein were proof-of-concept studies designed to illustrate the unique capabilities of ToF-SIMS, rather than studies that used feedback from ToF-SIMS to advance fundamental polymer science. This reflects the fact that ToF-SIMS is not yet a mainstream tool for polymer characterization in academia. However, there are several reasons to expect that ToF-SIMS will become more prevalent in the polymer science literature: First, recent advances in instrumentation (such as the introduction of gas cluster beams) have improved the ability to characterize polymer surfaces. Second, the wealth of proof-of-concept studies have established the feasibility of using ToF-SIMS analysis to inform a range of critical research areas, including polymers for energy conversion/storage and polymer-based composites. Finally, these instruments are becoming more widely available through shared facilities at universities and national laboratories.

There are characterization needs in polymer science where ToF-SIMS could be very valuable. As an example, studies have shown that ToF-SIMS depth profiling can probe penetrant diffusion in glassy polymers[102] as well as interdiffusion of polymers and small molecules[154]. The key advantage of using ToF-SIMS for diffusion studies is the intrinsic chemical contrast, which is particularly important when probing materials with complex chemical motifs. We envision that this method could be applied toward studies of

ion/molecular diffusion through membranes, diffusion of dopants in polymer semiconductors, and polymer-polymer interdiffusion at junctions. A challenge with such experiments is optimizing (and quantifying) the depth resolution, as this depends on the choice of ion beam for sputtering and its energy,[156] as well as the type of material being sputtered and its thickness. Furthermore, as the ToF-SIMS signal associated with a constituent is not always proportional to its concentration, this relationship must be quantified in order to model the shape of the diffusion front and calculate a diffusivity. Another opportunity for ToF-SIMS is to provide feedback for combinatorial materials science[71,157–159], such as characterization of "gradient surfaces".[160] The use of gradients is well-established for rapid screening of polymer blend morphologies[161], dispersion of fillers in polymer composites[162], surface chemistry and wettability for block copolymer self-assembly[159,163], and composition of mixed polyelectrolyte brushes for responsive surfaces[164]. Both the spectral analysis and imaging modes are quite fast, and all ToF-SIMS instruments have motorized stages, so one could easily acquire data at different positions along a gradient. It is worth noting that gradients often include the pure materials at each end, allowing one to acquire valuable reference spectra from the same sample.

ToF-SIMS also has unique capabilities for the study of polymeric biomaterials and hybrid materials. ToF-SIMS is capable of label-free analysis, which enables detection of specific biomarkers on a surface or in a sample. Recent work has extended the capabilities of ToF-SIMS to significantly enhance the mass resolving power using an Orbitrap analyzer.[165] The method is compatible with the other features of ToF-SIMS (focused ion beam, depth profiling), and it was applied for single-cell chemical imaging and metabolic profiling[166]. This capability could be useful for analysis of cellular scaffolds and polymers at the interface with cells and tissue, although it is rather specialized and not yet widely available. Recent studies of hybrid materials have taken advantage of the capability of ToF-SIMS to detect both elemental and molecular fragments to study electrode-electrolyte interfaces[167,168], degradation processes[138], and stratification near interfaces [148–150], but a broader range of applications could benefit from similar studies. This includes studies of polymeric membranes and solid electrolytes for energy storage and other electrochemical applications.

Finally, we note that ToF-SIMS can probe the composition of buried structures/interfaces by imaging cross-sections or depth profiling. As an example, ToF-SIMS was recently applied to chemically image cross-sections of two 17th century paintings by Nicolas Poussin in order to determine the binding medium used. The results obtained by ToF-SIMS suggested that an oil-based binder rather than an egg-based binder was likely used[169]. The data from ToF-SIMS depth profiling are complementary to those acquired from workhorse characterization tools such as XRR and NR, although the depth resolution is poorer. There may be opportunities to use the "real-space" data from ToF-SIMS to reduce uncertainty in the analysis of reciprocal-space data from scattering and reflectivity.

Acknowledgments

The authors acknowledge funding from the National Science Foundation under Award Nos. CMMI-1934061 (to University of Tennessee),CMMI-1934045 (to Rice University) and CBET-1626418 (to Rice University).

[1] J. S. Fletcher *Biointerphases*, **2015**, 10, 018902.
[2] A. Karen, N. Man, T. Shibamori, K. Takahashi *Applied Surface Science*, **2003**, 203–204, 541–546.
[3] J. P. Hofmann, M. Rohnke, B. M. Weckhuysen *Physical Chemistry Chemical Physics*, **2014**, 16, 5465–5474.
[4] V. S. Smentkowski, M. R. Keenan, H. Arlinghaus *Surface Science*, **2016**, 652, 39–45.
[5] A. A. Galuska *Surface and Interface Analysis*, **1997**, 25, 1–4.
[6] J. C. Vickerman, I. S. Gilmore Surface Analysis: The Principal Techniques, John Wiley & Sons, **2011**.
[7] J. C. Vickerman, D. Briggs ToF-SIMS: Materials Analysis by Mass Spectrometry, IM Publications, **2013**.
[8] S. Fearn An Introduction to Time-of-Flight Secondary Ion Mass Spectrometry (ToF-SIMS) and its Application to Materials Science, Morgan & Claypool, **2015**.
[9] R. N. S. Sodhi *The Analyst*, **2004**, 129, 483–487.
[10] J. S. Fletcher, J. C. Vickerman *Anal. Chem.*, **2013**, 85, 610–639.
[11] A. Benninghoven *Angewandte Chemie International Edition in English*, **1994**, 33, 1023–1043.
[12] D. M. Hercules *Journal of Molecular Structure*, **1993**, 292, 49–63.
[13] N. D. Treat, M. A. Brady, G. Smith, M. F. Toney, E. J. Kramer, C. J. Hawker, M. L. Chabinyc *Advanced Energy Materials*, **2011**, 1, 82–89.
[14] A. Brown, J. A. van den Berg, J. C. Vickerman *Surface and Interface Analysis*, **1986**, 9, 309–317.
[15] H. Y. Mou, S. Wu, P. Fardim *BioResources*, **2016**, 11, 5581–5599.
[16] N. P. Lockyer, J. C. Vickerman *Applied Surface Science*, **2004**, 231–232, 377–384.
[17] T. J. Barnes, I. M. Kempson, C. A. Prestidge *International Journal of Pharmaceutics*, **2011**, 417, 61–69.
[18] A. M. Belu, D. J. Graham, D. G. Castner *Biomaterials*, **2003**, 24, 3635–3653.
[19] B. Johansson *Surface and Interface Analysis*, **2006**, 38, 1401–1412.
[20] S. Fearn *Materials Science and Technology*, **2015**, 31, 148–161.
[21] A. D. Appelhans, J. E. Delmore *Anal. Chem.*, **1989**, 61, 1087–1093.
[22] J. Brison, S. Muramoto, D. G. Castner *J. Phys. Chem. C*, **2010**, 114, 5565–5573.
[23] S. Ninomiya, K. Ichiki, H. Yamada, Y. Nakata, T. Seki, T. Aoki, J. Matsuo *Rapid Communications in Mass Spectrometry*, **2009**, 23, 3264–3268.
[24] A. G. Shard, R. Havelund, M. P. Seah, S. J. Spencer, I. S. Gilmore, N. Winograd, D. Mao, T. Miyayama, E. Niehuis, D. Rading, R. Moellers *Anal. Chem.*, **2012**, 84, 7865–7873.
[25] Z. Postawa *Applied Surface Science*, **2004**, 231–232, 22–28.
[26] I. Yamada, J. Matsuo, N. Toyoda *Nuclear Instruments and Methods in Physics Research Section B: Beam Interactions with Materials and Atoms*, **2003**, 206, 820–829.
[27] F. Kötter, A. Benninghoven *Applied Surface Science*, **1998**, 133, 47–57.
[28] S. C. C. Wong, R. Hill, P. Blenkinsopp, N. P. Lockyer, D. E. Weibel, J. C. Vickerman *Applied Surface Science*, **2003**, 203–204, 219–222.
[29] J. Bailey, R. Havelund, A. G. Shard, I. S. Gilmore, M. R. Alexander, J. S. Sharp, D. J. Scurr *ACS Appl. Mater. Interfaces*, **2015**, 7, 2654–2659.
[30] M. P. Seah, S. J. Spencer, R. Havelund, I. S. Gilmore, A. G. Shard *Analyst*, **2015**, 140, 6508–6516.
[31] K. Shen, A. Wucher, N. Winograd *J. Phys. Chem. C*, **2015**, 119, 15316–15324.

[32] R. Havelund, M. P. Seah, I. S. Gilmore *Surface and Interface Analysis*, **2019**, 51, 1332–1341.
[33] R. Havelund, M. P. Seah, I. S. Gilmore *J. Phys. Chem. B*, **2016**, 120, 2604–2611.
[34] T. Terlier, G. Zappalà, C. Marie, D. Leonard, J.-P. Barnes, A. Licciardello *Anal. Chem.*, **2017**, 89, 6984–6991.
[35] P. Sjövall, D. Rading, S. Ray, L. Yang, A. G. Shard *J. Phys. Chem. B*, **2010**, 114, 769–774.
[36] B. Czerwinski, A. Delcorte *J. Phys. Chem. C*, **2013**, 117, 3595–3604.
[37] Y. Yokoyama, T. Kawashima, M. Ohkawa, H. Iwai, S. Aoyagi *Surface and Interface Analysis*, **2015**, 47, 439–446.
[38] C. W. T. Bulle-Lieuwma, W. J. H. van Gennip, J. K. J. van Duren, P. Jonkheijm, R. A. J. Janssen, J. W. Niemantsverdriet *Applied Surface Science*, **2003**, 203–204, 547–550.
[39] O. Roling, K. De Bruycker, B. Vonhören, L. Stricker, M. Körsgen, H. F. Arlinghaus, B. J. Ravoo, F. E. Du Prez *Angewandte Chemie International Edition*, **2015**, 54, 13126–13129.
[40] K. Miyagi, H. Mei, T. Terlier, G. E. Stein, R. Verduzco *Macromolecules*, **2020**, 53, 6720–6730.
[41] H. Mei, T. S. Laws, J. P. Mahalik, J. Li, A. H. Mah, T. Terlier, P. Bonnesen, D. Uhrig, R. Kumar, G. E. Stein, R. Verduzco *Macromolecules*, **2019**.
[42] M. Hernández-Guerrero, M. H. Stenzel *Polym. Chem.*, **2012**, 3, 563–577.
[43] K. Gajos, K. Awsiuk, A. Budkowski *Colloid Polym Sci*, **2020**.
[44] N. G. Welch, R. M. T. Madiona, T. B. Payten, C. D. Easton, L. Pontes-Braz, N. Brack, J. A. Scoble, B. W. Muir, P. J. Pigram *Acta Biomaterialia*, **2017**, 55, 172–182.
[45] S. Liu, L.-T. Weng, C.-M. Chan, L. Li, N. K. Ho, M. Jiang *Surface and Interface Analysis*, **2001**, 31, 745–753.
[46] J. L. S. Lee, I. S. Gilmore, M. P. Seah, A. P. Levick, A. G. Shard *Surface and Interface Analysis*, **2012**, 44, 238–245.
[47] M. A. Robinson, D. J. Graham, D. G. Castner *Anal. Chem.*, **2012**, 84, 4880–4885.
[48] Q. P. Vanbellingen, N. Elie, M. J. Eller, S. Della-Negra, D. Touboul, A. Brunelle *Rapid Communications in Mass Spectrometry*, **2015**, 29, 1187–1195.
[49] G. E. Stein, J. A. Liddle, A. L. Aquila, E. M. Gullikson *Macromolecules*, **2010**, 43, 433–441.
[50] P. M. Thompson *Analytical Chemistry*, **1991**, 63, 2447–2456.
[51] X. Vanden Eynde, P. Bertrand *Applied Surface Science*, **1999**, 141, 1–20.
[52] X. Vanden Eynde, P. Bertrand, J. Penelle *Macromolecules*, **2000**, 33, 5624–5633.
[53] L. Li, C.-M. Chan, L.-T. Weng, M.-L. Xiang, M. Jiang *Macromolecules*, **1998**, 31, 7248–7255.
[54] A. Priebe, T. Xie, G. Bürki, L. Pethö, J. Michler *Journal of Analytical Atomic Spectrometry*, **2020**, 35, 1156–1166.
[55] L.-T. Weng, K.-M. Ng, Z. L. Cheung, Y. Lei, C.-M. Chan *Surface and Interface Analysis*, **2006**, 38, 32–43.
[56] L. T. Weng, P. Bertrand, W. Lauer, R. Zimmer, S. Busetti *Surface and Interface Analysis*, **1995**, 23, 879–886.
[57] L. Li, C.-M. Chan, S. Liu, L. An, K.-M. Ng, L.-T. Weng, K.-C. Ho *Macromolecules*, **2000**, 33, 8002–8005.
[58] A. H. Mah, T. Laws, W. Li, H. Mei, C. C. Brown, A. Ievlev, R. Kumar, R. Verduzco, G. E. Stein *Macromolecules*, **2019**, 52, 1526–1535.
[59] L. T. Weng, C.-M. Chan *Applied Surface Science*, **2003**, 203–204, 532–537.
[60] A. G. Shard, A. Rafati, R. Ogaki, J. L. S. Lee, S. Hutton, G. Mishra, M. C. Davies, M. R. Alexander *J. Phys. Chem. B*, **2009**, 113, 11574–11582.

[61] A. G. Shard, S. J. Spencer, S. A. Smith, R. Havelund, I. S. Gilmore *International Journal of Mass Spectrometry*, **2015**, 377, 599–609.
[62] A. Delcorte, P. Bertrand *Applied Surface Science*, **2004**, 231–232, 250–255.
[63] M. Inoue, A. Murase *Surface and Interface Analysis*, **2005**, 37, 1111–1114.
[64] Y. Gao *Journal of Applied Physics*, **1988**, 64, 3760–3762.
[65] Y. Gao, Y. Marie, F. Saldi, H.-N. Migeon *International Journal of Mass Spectrometry and Ion Processes*, **1995**, 143, 11–18.
[66] G. Karras, N. P. Lockyer *J. Am. Soc. Mass Spectrom.*, **2014**, 25, 832–840.
[67] A. Kucher, L. M. Jackson, J. O. Lerach, A. N. Bloom, N. J. Popczun, A. Wucher, N. Winograd *Anal. Chem.*, **2014**, 86, 8613–8620.
[68] G. F. Trindade, M.-L. Abel, J. F. Watts *Chemometrics and Intelligent Laboratory Systems*, **2018**, 182, 180–187.
[69] B. J. Tyler, G. Rayal, D. G. Castner *Biomaterials*, **2007**, 28, 2412–2423.
[70] D. J. Graham, D. G. Castner *Biointerphases*, **2012**, 7, 49.
[71] A. J. Urquhart, D. G. Anderson, M. Taylor, M. R. Alexander, R. Langer, M. C. Davies *Advanced Materials*, **2007**, 19, 2486–2491.
[72] G. L. Fisher, A. L. Bruinen, N. Ogrinc Potočnik, J. S. Hammond, S. R. Bryan, P. E. Larson, R. M. A. Heeren *Anal. Chem.*, **2016**, 88, 6433–6440.
[73] E. de Hoffmann *Journal of Mass Spectrometry*, **1996**, 31, 129–137.
[74] A. R. Johnson, E. E. Carlson *Anal. Chem.*, **2015**, 87, 10668–10678.
[75] A. J. Taylor, D. J. Graham, D. G. Castner *Analyst*, **2015**, 140, 6005–6014.
[76] T. Wirtz, Y. Fleming, M. Gerard, U. Gysin, T. Glatzel, E. Meyer, U. Wegmann, U. Maier, A. H. Odriozola, D. Uehli *Review of Scientific Instruments*, **2012**, 83, 063702.
[77] L. Bernard, J. Heier, W. Paul, H. J. Hug *Nuclear Instruments and Methods in Physics Research Section B: Beam Interactions with Materials and Atoms*, **2014**, 339, 85–90.
[78] S. Iida, D. M. Carr, G. L. Fisher, T. Miyayama *Journal of Vacuum Science & Technology B*, **2018**, 36, 03F107.
[79] F. Vollnhals, T. Wirtz *Anal. Chem.*, **2018**, 90, 11989–11995.
[80] N. Becker, T. Wirtz, H.-N. Migeon *Surface and Interface Analysis*, **2011**, 43, 413–416.
[81] R. Hill, P. Blenkinsopp, S. Thompson, J. Vickerman, J. S. Fletcher *Surface and Interface Analysis*, **2011**, 43, 506–509.
[82] Y. Zhou, J. Yao, Y. Ding, J. Yu, X. Hua, J. E. Evans, X. Yu, D. B. Lao, D. J. Heldebrant, S. K. Nune, B. Cao, M. E. Bowden, X.-Y. Yu, X.-L. Wang, Z. Zhu *J. Am. Soc. Mass Spectrom.*, **2016**, 27, 2006–2013.
[83] K. Matyjaszewski, P. J. Miller, N. Shukla, B. Immaraporn, A. Gelman, B. B. Luokala, T. M. Siclovan, G. Kickelbick, T. Vallant, H. Hoffmann, T. Pakula *Macromolecules*, **1999**, 32, 8716–8724.
[84] R. Barbey, L. Lavanant, D. Paripovic, N. Schüwer, C. Sugnaux, S. Tugulu, H.-A. Klok *Chem. Rev.*, **2009**, 109, 5437–5527.
[85] Q. Peng, D. M. Y. Lai, E. T. Kang, K. G. Neoh *Macromolecules*, **2006**, 39, 5577–5582.
[86] A. S. Schulz, H. Gojzewski, J. Huskens, W. L. Vos, G. J. Vancso *Polymers for Advanced Technologies*, **2018**, 29, 806–813.
[87] U. Oran, S. Swaraj, A. Lippitz, W. E. S. Unger *Plasma Processes and Polymers*, **2006**, 3, 288–298.
[88] N. Hadjesfandiari, M. Weinhart, J. N. Kizhakkedathu, R. Haag, D. E. Brooks *Advanced Healthcare Materials*, **2018**, 7, 1700839.

[89] J. Kim, H. K. Shon, D. Jung, D. W. Moon, S. Y. Han, T. G. Lee *Anal. Chem.*, **2005**, 77, 4137–4141.
[90] J. Kim, D. Jung, Y. Park, Y. Kim, D. W. Moon, T. G. Lee *Applied Surface Science*, **2007**, 253, 4112–4118.
[91] G. Widawski, M. Rawiso, B. François *Nature*, **1994**, 369, 387–389.
[92] P. Escalé, L. Rubatat, L. Billon, M. Save *European Polymer Journal*, **2012**, 48, 1001–1025.
[93] S. Yunus, A. Delcorte, C. Poleunis, P. Bertrand, A. Bolognesi, C. Botta *Advanced Functional Materials*, **2007**, 17, 1079–1084.
[94] F. Galeotti, V. Calabrese, M. Cavazzini, S. Quici, C. Poleunis, S. Yunus, A. Bolognesi *Chem. Mater.*, **2010**, 22, 2764–2769.
[95] M. Dubey, K. Emoto, F. Cheng, L. J. Gamble, H. Takahashi, D. W. Grainger, D. G. Castner *Surface and Interface Analysis*, **2009**, 41, 645–652.
[96] X. Du, L. Li, J. Li, C. Yang, N. Frenkel, A. Welle, S. Heissler, A. Nefedov, M. Grunze, P. A. Levkin *Advanced Materials*, **2014**, 26, 8029–8033.
[97] H. Lee, S. M. Dellatore, W. M. Miller, P. B. Messersmith *Science*, **2007**, 318, 426–430.
[98] S. J. Hinder, C. Lowe, J. T. Maxted, J. F. Watts *Surface and Interface Analysis*, **2004**, 36, 1575–1581.
[99] W. Guo, C. M. Reese, L. Xiong, P. K. Logan, B. J. Thompson, C. M. Stafford, A. V. Ievlev, B. S. Lokitz, O. S. Ovchinnikova, D. L. Patton *Macromolecules*, **2017**, 50, 8670–8677.
[100] Y. Kim, Y. Lee, S. Han, K.-J. Kim *Surface and Coatings Technology*, **2006**, 200, 4763–4769.
[101] P. Rupper, M. Vandenbossche, L. Bernard, D. Hegemann, M. Heuberger *Langmuir*, **2017**, 33, 2340–2352.
[102] C. M. Bottoms, T. Terlier, G. E. Stein, M. Doxastakis *Macromolecules*, **2021**, 54, 1912–1925.
[103] H. Mei, A. H. Mah, Z. Hu, Y. Li, T. Terlier, G. E. Stein, R. Verduzco *ACS Macro Lett.*, **2020**, 9, 1135–1142.
[104] C. Zhou, D. Sun, R. Garcia, F. A. Stevie *Analytical Methods*, **2018**, 10, 2444–2449.
[105] H. Mei, A. H. Mah, Z. Hu, Y. Li, T. Terlier, G. E. Stein, R. Verduzco *ACS Macro Lett.*, **2020**, 9, 1135–1142.
[106] X. Ren, L.-T. Weng, C.-M. Chan, K.-M. Ng *Anal. Chem.*, **2012**, 84, 8497–8504.
[107] D. Cossement, R. Gouttebaron, V. Cornet, P. Viville, M. Hecq, R. Lazzaroni *Applied Surface Science*, **2006**, 252, 6636–6639.
[108] C. M. Dekeyser, S. Biltresse, J. Marchand-Brynaert, P. G. Rouxhet, Ch. C. Dupont-Gillain *Polymer*, **2004**, 45, 2211–2219.
[109] G. F. Trindade, M.-L. Abel, C. Lowe, R. Tshulu, J. F. Watts *Analytical Chemistry*, **2018**, 90, 3936–3941.
[110] T. Kono, E. Iwase, Y. Kanamori *Applied Surface Science*, **2008**, 255, 997–1000.
[111] T. Miyasaka, T. Ikemoto, T. Kohno *Applied Surface Science*, **2008**, 255, 1576–1579.
[112] S. Ravati, S. Poulin, K. Piyakis, B. D. Favis *Polymer*, **2014**, 55, 6110–6123.
[113] S.-F. Wang, X. Li, R. L. Agapov, C. Wesdemiotis, M. D. Foster *ACS Macro Lett.*, **2012**, 1, 1024–1027.
[114] C. M. Mahoney, J. Yu, A. Fahey, J. A. Gardella *Applied Surface Science*, **2006**, 252, 6609–6614.
[115] F. Awaja, P. J. Pigram *Polymer Degradation and Stability*, **2009**, 94, 651–658.

[116] F. Awaja, J. B. Moon, M. Gilbert, S. Zhang, C. G. Kim, P. J. Pigram *Polymer Degradation and Stability*, **2011**, 96, 1301–1309.
[117] N. E. Zafeiropoulos, P. E. Vickers, C. A. Baillie, J. F. Watts *Journal of Materials Science*, **2003**, 38, 3903–3914.
[118] C. S. R. Freire, A. J. D. Silvestre, C. Pascoal Neto, A. Gandini, P. Fardim, B. Holmbom *Journal of Colloid and Interface Science*, **2006**, 301, 205–209.
[119] J. T. Cherian, D. G. Castner *Surface and Interface Analysis*, **2000**, 29, 729–734.
[120] R. Mason, J. Emerson, J. T. Koberstein *The Journal of Adhesion*, **2004**, 80, 119–143.
[121] D. K. Chattopadhyay, K. V. S. N. Raju *Progress in Polymer Science*, **2007**, 32, 352–418.
[122] Q. Benard, M. Fois, M. Grisel, P. Laurens, F. Joubert *Journal of Thermoplastic Composite Materials*, **2009**, 22, 51–61.
[123] Q. Bénard, M. Fois, M. Grisel *Composites Part A: Applied Science and Manufacturing*, **2005**, 36, 1562–1568.
[124] M. J. Gilbert, F. Awaja, G. L. Kelly, B. L. Fox, R. Brynolf, P. J. Pigram *Surface and Interface Analysis*, **2011**, 43, 856–864.
[125] N. Karar, T. K. Gupta *Vacuum*, **2015**, 111, 119–123.
[126] Z. Liu, K. Parvez, R. Li, R. Dong, X. Feng, K. Müllen *Advanced Materials*, **2015**, 27, 669–675.
[127] W. K. Chee, H. N. Lim, N. M. Huang, I. Harrison *RSC Adv.*, **2015**, 5, 68014–68051.
[128] B. Brennan, S. J. Spencer, N. A. Belsey, T. Faris, H. Cronin, S. R. P. Silva, T. Sainsbury, I. S. Gilmore, Z. Stoeva, A. J. Pollard *Applied Surface Science*, **2017**, 403, 403–412.
[129] C. Yang, Y.-T. Xie, M. M.-F. Yuen, B. Xu, B. Gao, X. Xiong, C. P. Wong *Advanced Functional Materials*, **2010**, 20, 2580–2587.
[130] K. Chatterjee, S. Banerjee, D. Chakravorty *Europhys. Lett.*, **2004**, 66, 592–598.
[131] N. P. Bradshaw, S. Y. Severt, Z. Wang, C. V. Fengel, J. D. Larson, Z. Zhu, A. R. Murphy, J. M. Leger. *Synthetic Metals*, **2015**, 209, 490–495.
[132] E. Peled, S. Menkin *J. Electrochem. Soc.*, **2017**, 164, A1703.
[133] T. Okumura, S. Nishimura *Journal of The Electrochemical Society*, **2018**, 165, A802–A808.
[134] A. Konarov, Z. Bakenov, H. Yashiro, Y.-K. Sun, S.-T. Myung *Journal of Power Sources*, **2017**, 355, 140–146.
[135] S. K. Hau, H.-L. Yip, A. K.-Y. Jen *Polymer Reviews*, **2010**, 50, 474–510.
[136] A. Sharma, S. E. Watkins, D. A. Lewis, G. Andersson *Solar Energy Materials and Solar Cells*, **2011**, 95, 3251–3255.
[137] A. Sharma, G. Andersson, D. A. Lewis *Phys. Chem. Chem. Phys.*, **2011**, 13, 4381–4387.
[138] J. Kettle, H. Waters, Z. Ding, M. Horie, G. C. Smith *Solar Energy Materials and Solar Cells*, **2015**, 141, 139–147.
[139] A. Fedorková, R. Oriňáková, A. Oriňák, A. Heile, H.-D. Wiemhöfer, H. F. Arlinghaus *Solid State Sciences*, **2011**, 13, 824–830.
[140] B. Czerwinski, A. Delcorte *J. Phys. Chem. C*, **2013**, 117, 3595–3604.
[141] T. Mouhib, C. Poleunis, N. Wehbe, J. J. Michels, Y. Galagan, L. Houssiau, P. Bertrand, A. Delcorte *Analyst*, **2013**, 138, 6801–6810.
[142] V. S. Smentkowski, G. Zorn, A. Misner, G. Parthasarathy, A. Couture, E. Tallarek, B. Hagenhoff *Journal of Vacuum Science & Technology A*, **2013**, 31, 030601.
[143] C. Fleischmann, T. Conard, R. Havelund, A. Franquet, C. Poleunis, E. Voroshazi, A. Delcorte, W. Vandervorst *Surface and Interface Analysis*, **2014**, 46, 54–57.

[144] S. Surana, T. Conard, C. Fleischmann, J. G. Tait, J. P. Bastos, E. Voroshazi, R. Havelund, M. Turbiez, P. Louette, A. Felten, C. Poleunis, A. Delcorte, W. Vandervorst *J. Phys. Chem. C*, **2016**, 120, 28074–28082.
[145] A. C. Arias *Journal of Macromolecular Science, Part C*, **2006**, 46, 103–125.
[146] Y. Yan, X. Liu, T. Wang *Advanced Materials*, **2017**, 29, 1601674.
[147] L. Huang, G. Wang, W. Zhou, B. Fu, X. Cheng, L. Zhang, Z. Yuan, S. Xiong, L. Zhang, Y. Xie, A. Zhang, Y. Zhang, W. Ma, W. Li, Y. Zhou, E. Reichmanis, Y. Chen *ACS Nano*, **2018**, 12, 4440–4452.
[148] R. Sun, J. Guo, Q. Wu, Z. Zhang, W. Yang, J. Guo, M. Shi, Y. Zhang, S. Kahmann, L. Ye, X. Jiao, M. A. Loi, Q. Shen, H. Ade, W. Tang, C. J. Brabec, J. Min *Energy Environ. Sci.*, **2019**, 12, 3118–3132.
[149] Y. Murat, E. Langer, J.-P. Barnes, J.-Y. Laurent, G. Wantz, L. Hirsch, T. Maindron *Organic Electronics*, **2017**, 48, 377–381.
[150] B. Cao, X. He, C. R. Fetterly, B. C. Olsen, E. J. Luber, J. M. Buriak *ACS Applied Materials & Interfaces*, **2016**, 8, 18238–18248.
[151] L. He, C. Jiang, H. Wang, D. Lai, Y. Heng Tan, C. Seng Tan, Rusli *Appl. Phys. Lett.*, **2012**, 100, 103104.
[152] J. P. Thomas, L. Zhao, M. Abd-Ellah, N. F. Heinig, K. T. Leung *Anal. Chem.*, **2013**, 85, 6840–6845.
[153] K. Norrman, M. V. Madsen, S. A. Gevorgyan, F. C. Krebs *J. Am. Chem. Soc.*, **2010**, 132, 16883–16892.
[154] M. Ghasemi, N. Balar, Z. Peng, H. Hu, Y. Qin, T. Kim, J. J. Rech, M. Bidwell, W. Mask, I. McCulloch, W. You, A. Amassian, C. Risko, B. T. O'Connor, H. Ade *Nature Materials*, **2021**, 20, 525–532.
[155] G. Zhang, J. Zhao, P. C. Y. Chow, K. Jiang, J. Zhang, Z. Zhu, J. Zhang, F. Huang, H. Yan *Chem. Rev.*, **2018**, 118, 3447–3507.
[156] C. Noël, Y. Busby, N. Mine, L. Houssiau *J. Am. Soc. Mass Spectrom.*, **2019**, 30, 1537–1544.
[157] A. L. Hook, D. J. Scurr *Surface and Interface Analysis*, **2016**, 48, 226–236.
[158] A. D. Celiz, J. G. W. Smith, A. K. Patel, R. Langer, D. G. Anderson, D. A. Barrett, L. E. Young, M. C. Davies, C. Denning, M. R. Alexander *Biomater. Sci.*, **2014**, 2, 1604–1611.
[159] A. P. Smith, A. Sehgal, J. F. Douglas, A. Karim, E. J. Amis *Macromolecular Rapid Communications*, **2003**, 24, 131–135.
[160] J. Genzer, R. R. Bhat *Langmuir*, **2008**, 24, 2294–2317.
[161] J. C. Meredith, A. Karim, E. J. Amis *Macromolecules*, **2000**, 33, 5760–5762.
[162] J. W. Gilman, S. Bourbigot, J. R. Shields, M. Nyden, T. Kashiwagi, R. D. Davis, D. L. Vanderhart, W. Demory, C. A. Wilkie, A. B. Morgan, J. Harris, R. E. Lyon *Journal of Materials Science*, **2003**, 38, 4451–4460.
[163] J. N. L. Albert, M. J. Baney, C. M. Stafford, J. Y. Kelly, T. H. Epps *ACS Nano*, **2009**, 3, 3977–3986.
[164] L. Ionov, N. Houbenov, A. Sidorenko, M. Stamm, I. Luzinov, S. Minko *Langmuir*, **2004**, 20, 9916–9919.
[165] A. M. Kotowska, G. F. Trindade, P. M. Mendes, P. M. Williams, J. W. Aylott, A. G. Shard, M. R. Alexander, D. J. Scurr *Nature Communications*, **2020**, 11, 5832.

[166] M. K. Passarelli, A. Pirkl, R. Moellers, D. Grinfeld, F. Kollmer, R. Havelund, C. F. Newman, P. S. Marshall, H. Arlinghaus, M. R. Alexander, A. West, S. Horning, E. Niehuis, A. Makarov, C. T. Dollery, I. S. Gilmore *Nature Methods*, **2017**, 14, 1175–1183.
[167] A. K. Haridas, Q. A. Nguyen, T. Terlier, R. Blaser, S. L. Biswal *ACS Appl. Mater. Interfaces*, **2021**, 13, 2662–2673.
[168] F. Hao, X. Chi, Y. Liang, Y. Zhang, R. Xu, H. Guo, T. Terlier, H. Dong, K. Zhao, J. Lou, Y. Yao *Joule*, **2019**, 3, 1349–1359.
[169] C. Bouvier, H. Glanville, L. de Viguerie, C. Merucci, P. Walter, A. Brunelle *Anal. Chem.*, **2021**, 93, 4463–4471.

Table of Contents Entry

This Review describes how time-of-flight secondary ion mass spectrometry (ToF-SIMS) is used to measure the chemical composition of polymer surfaces and interfaces. This technique is introduced through case studies that highlight the three principal modes of operation (spectral analysis, imaging and depth profiling) as applied to characterization of polymer thin films, polymer blends, composites, and electronic materials. Strategies for experimental design and data analysis are also discussed.

Hao Mei, Travis S. Laws, Tanguy Terlier, Rafael Verduzco*, Gila E. Stein*

Title: Characterization of Polymeric Surfaces and Interfaces using Time-of-Flight Secondary Ion Mass Spectrometry